Analysis of Stability and Dispersion in a Finite Element Method for Debye and Lorentz Dispersive Media

H. T. Banks,[1] **V. A. Bokil,**[2] **N. L. Gibson**[2]
[1] *Center for Research in Scientific Computation, North Carolina State University, Raleigh, North Carolina 27695-8205*

[2] *Department of Mathematics, Oregon State University, Corvallis, Oregon 97331-4605*

Received 21 December 2006; accepted 30 April 2008
Published online in Wiley InterScience (www.interscience.wiley.com).
DOI 10.1002/num.20379

We study the stability properties of, and the phase error present in, a finite element scheme for Maxwell's equations coupled with a Debye or Lorentz polarization model. In one dimension we consider a second order formulation for the electric field with an ordinary differential equation for the electric polarization added as an auxiliary constraint. The finite element method uses linear finite elements in space for the electric field as well as the electric polarization, and a theta scheme for the time discretization. Numerical experiments suggest the method is unconditionally stable for both Debye and Lorentz models. We compare the stability and phase error properties of the method presented here with those of finite difference methods that have been analyzed in the literature. We also conduct numerical simulations that verify the stability and dispersion properties of the scheme. © 2008 Wiley Periodicals, Inc. Numer Methods Partial Differential Eq 00: 000–000, 2008

Keywords: Maxwell's equations; Debye; Lorentz; finite elements; FDTD; dissipation; dispersion

I. INTRODUCTION

Noninvasive interrogation of the interior of tissues and other materials by electromagnetic waves has important applications in various fields including medical imaging for the early detection of anomalies and nondestructive damage detection in aircraft [1, 2]. For example, microwave imaging for breast cancer detection is expected to be safe for the patient and has the potential to detect very small cancerous tumors in the breast [3]. This ability for detection is based on the difference in electrical properties of malignant and normal tissues. Biological tissue interactions with the fields are defined by their complex permittivity, which is a function of the various electric

Correspondence to: H. T. Banks, Center for Research in Scientific Computation, North Carolina State University, Raleigh, NC 27695-8205 (e-mail: htbanks@ncsu.edu)
Contract grant sponsor: U.S. Air Force Office of Scientific Research; contract grant number: AFOSR FA9550-04-1-0220
Contract grant sponsor: National Institute of Aerospace (NIA)
Contract grant sponsor: NASA; contract grant number: NIA/NCSU-03-01-2536-NC

and magnetic polarization mechanisms and conductivity of the biological medium. Similarly, nondestructive damage detection in materials for the detection of defects such as cracks is based upon the changes in the electrical properties that occur due to the presence of these defects. Thus, one aim of electromagnetic interrogation is the determination of the dielectric properties of the materials under investigation.

To computationally simulate these electromagnetic interrogation problems requires setting up a suitable inverse problem, which involves numerous forward simulations of the propagation of transient electromagnetic waves in lossy dispersive dielectrics, such as biological tissue. Hence, the development of accurate, consistent and stable discrete forward solvers is very important, as errors in the numerical solvers can result in inaccurate determination of the dielectric properties that determine the characteristics of the material being investigated.

The electric and magnetic fields inside a material are governed by the macroscopic Maxwell's equations along with constitutive laws that account for the response of the material to the electromagnetic field. In special cases Maxwell's equations can be reduced to a vector wave equation in the electric or magnetic fields. Numerical approximation algorithms of time-dependent wave equations and Maxwell's equations introduce error into the amplitude and speed of the propagating waves. These errors include *dissipation*, the dampening of some frequency modes, and *dispersion*, the frequency dependence of the phase velocity of numerical wave modes in the computational grid.

Dielectric materials have actual physical dispersion. The complex electric permittivity of a dielectric medium is frequency dependent (has dielectric dispersion). Thus, an appropriate discretization method should have a numerical dispersion that matches the model dispersion as closely as possible. Dielectric materials also have physical dissipation, or attenuation, which must also be correctly computed by a numerical method. In particular, if a method does not sufficiently damp initial disturbances, possibly due to round-off error, the method can become unstable. Certain algorithms have criteria based on discretization parameters to determine when it may be unstable; these are called *conditionally stable methods*.

The stability and dispersion properties for the finite difference time domain (FDTD) schemes applied to Maxwell's equations in free space are well known (see [4]). Additionally, different time domain finite element methods have also been devised for the numerical approximation of Maxwell's equations in free space (see [5, 6] and the references therein). While free space analyses for finite element and finite difference methods are well documented, stability and phase error analysis for dispersive dielectrics has been primarily focused on finite difference methods (see [4, 7] for standard second order methods and [8] for higher order schemes). The treatment for finite element methods has been limited to scalar-potential formulations to model dielectric dispersion at low frequencies ([9]), scalar Helmholtz equation ([10]), and in some cases, hybrid methods ([11]).

There are several FDTD extensions that have been developed to model electromagnetic pulse propagation in dispersive media. One technique is to add to Maxwell's equations a set of ODE's that relate the electric displacement $\vec{D}(t)$ to the electric field $\vec{E}(t)$ [12], or a set of ODE's that model the dynamic evolution of the macroscopic polarization vector $\vec{P}(t)$ driven by the electric field [13, 14]. Dielectric dispersion can be expressed in the time domain as a convolution integral involving the electric field and a causal susceptibility function. The recursive convolution method [15–17] uses a recursive technique to update the convolution representation of the constitutive law along with the FDTD time update of Maxwell's equations. There are other methods such as the Z-transform [18, 19] and the TLM method [20] that have also been used to model pulse propagation in dispersive media. Many of these methods have been compared and analyzed for their numerical errors and stability properties [7, 21–24].

In this article we study the properties of the discretized Maxwell's equations with Debye or Lorentz polarization, using a finite element method, in terms of numerical stability and dispersion analyses. We analyze one dimensional models to which we apply standard linear finite elements for the spatial discretization of the electric field and the polarization. Maxwell's equations are reduced to a wave equation in the electric field, and the constitutive law in the medium involves an ordinary differential equation that describes the dynamic evolution of the polarization driven by the electric field. The entire system is rewritten in first order form and time discretized using a theta scheme.

The numerical stability results for Debye and Lorentz media suggest that the extension of the finite element scheme for these media retain the unconditional stability property of the scheme in free space. We obtain information about the expected accuracy of the method from the construction of the dispersion relation which relates the numerical wave number k to the frequency ω for waves propagating in the finite element grid and then compare with the dispersion relation for the corresponding continuous model. We compare the stability and dispersion properties of the finite element method with those of finite difference methods analyzed in [7]. Such finite element methods have been used for the electromagnetic interrogation of dielectric media with a metal backing, for the determination of dielectric properties and geometrical dimensions of the medium [25], as well as for the detection of cracks in composite materials [26]. In [27], finite element methods were used to interrogate dielectric media with acoustic waves as virtual reflectors.

The Lax-Richtmyer theorem [28] states that the convergence of consistent difference schemes to initial value problems represented by PDE's is equivalent to stability. Thus, unconditional stability is a desirable property of temporal discretization schemes as it allows the choice of the time step to be determined by the physical dimensions of the problem, such as a relaxation time. The FDTD methods, however, are conditionally stable. As the stability condition is determined by the smallest cell size in the domain, the FDTD analysis of very fine geometric structures requires a large number of time iterations. In the finite element case unconditional stability allows us to choose the *Courant number*, which relates the time step to the mesh step size, to minimize the numerical phase error.

The numerical dispersion analysis shows that for accuracy we need to resolve the shortest time scale in the problem which agrees with the result obtained in [7]. This is reflected in the fact that the time step for simulating Debye media should be chosen to be about $O(10^{-3})\tau$, where τ is the relaxation time of the medium, whereas for Lorentz media, the time step should be chosen to be the minimum of $O(10^{-2})\tau$ and $O(10^{-2})\left(\frac{2\pi}{\omega_0}\right)$, where ω_0 is the resonance frequency of the medium.

We thus determine a guideline for users in which the time step is chosen to minimize the dissipation of the scheme and the Courant factor is chosen to minimize the phase error, providing good agreement between the exact and numerical complex permittivity. Finally, we present simulations that validate our results.

II. MODEL FORMULATION

We consider Maxwell's equations that govern the electric field $\vec{E}$ and the magnetic field $\vec{H}$ in a domain Ω from time 0 to T given as

$$\frac{\partial \vec{D}}{\partial t} + \vec{J} - \nabla \times \vec{H} = 0 \text{ in } (0,T) \times \Omega, \tag{2.1a}$$

$$\frac{\partial \vec{B}}{\partial t} + \nabla \times \vec{E} = 0 \text{ in } (0,T) \times \Omega, \tag{2.1b}$$

$$\nabla \cdot \vec{D} = 0 = \nabla \cdot \vec{B} \text{ in } (0,T) \times \Omega, \tag{2.1c}$$

$$\vec{E}(0,\vec{x}) = 0 = \vec{H}(0,\vec{x}) \text{ in } \Omega. \tag{2.1d}$$

The fields $\vec{D}, \vec{B}$ are the electric and magnetic flux densities respectively. All the fields in (2.1) are functions of position $\vec{x} = (x, y, z)$ and time t. We have $\vec{J} = \vec{J}_c + \vec{J}_s$, where $\vec{J}_c$ is a conduction current density and $\vec{J}_s$ is the source current density. However, we will assume $\vec{J}_c = 0$ in this paper, as we are interested in dielectrics with no free charges. Appropriate boundary conditions are added to system (2.1) to terminate the computational domain.

Constitutive relations, which relate the electric and magnetic fluxes $\vec{D}, \vec{B}$ to the electric and magnetic fields $\vec{E}, \vec{H}$ are added to these equations to make the system fully determined and to describe the response of a material to the electromagnetic fields. In free space, these constitutive relations are $\vec{D} = \epsilon_0 \vec{E}$, and $\vec{B} = \mu_0 \vec{H}$, where ϵ_0 and μ_0 are the permittivity and the permeability of free space, respectively, and are constant [29]. In general there are different possible forms for these constitutive relationships. In a frequency domain formulation of Maxwell's equations, these are usually converted to linear relationships between the dependent and independent quantities with frequency dependent coefficient parameters. We will consider the case of a dielectric in which magnetic effects are negligible. Thus, within the dielectric medium we have constitutive relations that relate the flux densities $\vec{D}, \vec{B}$ to the electric and magnetic fields, respectively, as

$$\vec{D} = \epsilon_0 \vec{E} + \vec{P}, \tag{2.2a}$$

$$\vec{B} = \mu_0 \vec{H}. \tag{2.2b}$$

In (2.2a), the quantity $\vec{P}$ is called the macroscopic electric polarization. (A discussion of the relationship between the macroscopic polarization and the microscopic material properties leading to distributions of relaxation times and other dielectric parameters in the constitutive laws can be found in [30].) Electric polarization may be defined as the electric field induced disturbance of the charge distribution in a region. This polarization may have an instantaneous component as well as delayed effects; the latter will usually have associated time constants called relaxation times which are denoted by τ. We define the instantaneous component of the polarization to be related to the electric field by means of the free space permittivity, ϵ_0, and a susceptibility χ. The remainder of the electric polarization, called the relaxation polarization, is denoted as $\vec{P}_{\mathrm{R}}$. Therefore, we have

$$\vec{P} = \vec{P}_{\mathrm{I}} + \vec{P}_{\mathrm{R}} = \epsilon_0 \chi \vec{E} + \vec{P}_{\mathrm{R}},$$

and hence the constitutive law (2.2a) becomes

$$\vec{D} = \epsilon_0 \epsilon_r \vec{E} + \vec{P}_{\mathrm{R}},$$

where $\epsilon_r = (1 + \chi)$ is the relative permittivity of the dielectric medium. We will henceforth denote $\vec{P}_{\mathrm{R}}$ by $\vec{P}$, as the instantaneous polarization will be absorbed into the dielectric constant ϵ_r. The following section defines the equations for polarization models of interest in this paper.

A. Models for Polarization

To describe the behavior of the media's relaxation polarization $\vec{P}$, one may use ordinary differential equation models derived from those that consider microscopic polarization mechanisms

such as dipole or orientational polarization (Debye), as well as ionic and electronic polarization (Lorentz), and other frequency dependent polarization mechanisms [31]. For more complex dielectric materials, a simple Debye or Lorentz polarization model is often not adequate to characterize the dispersive behavior of the material. One can then turn to combinations of Debye, Lorentz, or even more general nth order mechanisms [25] as well as Cole-Cole type (fractional order derivative) models [32]. Additionally, materials may be represented by a distribution of the associated time constants or even a distribution of polarization mechanisms (see [30, 33]). In this report we concentrate our analysis on single pole Debye and Lorentz polarization models.

Debye Model The macroscopic differential equation for the *Debye model* for *orientational* or *dipolar polarization* is given by

$$\tau \frac{\partial \vec{P}}{\partial t} + \vec{P} = \epsilon_0(\epsilon_s - \epsilon_\infty)\vec{E}. \tag{2.3}$$

Here ϵ_s is the static relative permittivity. The presence of instantaneous polarization is accounted for in this case by the coefficient $\epsilon_r = \epsilon_\infty$ in the electric flux equation (2.3). The electric polarization, less the part included in the instantaneous polarization, is seen to be a decaying exponential with relaxation parameter τ, which is driven by the electric field. This model was first proposed by Debye [34] to model the behavior of materials that possess permanent dipole moments. The magnitude of the polarization term $\vec{P}$ represents the degree of alignment of these individual moments and is based on a uniformity assumption at the molecular level (see [30]). The choice of coefficients in (2.3) gives a physical interpretation to ϵ_s and ϵ_∞ as the relative permittivities of the medium in the limit of the static field and very high frequencies, respectively. In the static case, we have $\vec{P}_t = 0$, so that $\vec{P} = \epsilon_0(\epsilon_s - \epsilon_\infty)\vec{E}$ and $\vec{D} = \epsilon_0\epsilon_s\vec{E}$. For very high frequencies, $\tau\vec{P}_t$ dominates $\vec{P}$ so that $\vec{P} \approx 0$ and $\vec{D} = \epsilon_0\epsilon_\infty\vec{E}$ (thus the notation of ∞).

The Debye model is most often used to model electromagnetic wave interactions with water-based substances, such as biological materials. In particular, biological tissue is well represented by multi-pole Debye models, by accounting for permanent dipole moments in the water. The Debye model has other physical characteristics which make it attractive from an analytical point of view (for details, see [21]).

Lorentz Model The *Lorentz model* for *electronic* polarization in differential form is represented with the second order equation:

$$\frac{\partial^2 \vec{P}}{\partial t^2} + \frac{1}{\tau}\frac{\partial \vec{P}}{\partial t} + \omega_0^2 \vec{P} = \epsilon_0\epsilon_d\omega_0^2\vec{E}, \tag{2.4}$$

where $\epsilon_d = \epsilon_s - \epsilon_\infty$ and ω_0 is the resonance frequency of the material.

The Lorentz model is formulated by modeling the atomic structure of the material as a damped vibrating system representing a deformable electron cloud at the atomic level [25]. Applying classical Newtonian laws of motion, we find that the displacement of the outermost shell of the atom satisfies a second-order ordinary differential equation [21].

B. Reduction to One Dimension

The electric field is assumed to be polarized to have oscillations in the x–z plane only, as described in [25]. Restricting the problem to one dimension, we can write the electric and magnetic fields,

$\vec{E}$ and $\vec{H}$ respectively, as follows

$$\vec{E}(t,\vec{x}) = \hat{i}\,E(t,z)$$
$$\vec{H}(t,\vec{x}) = \hat{j}\,H(t,z),$$

so that we are only concerned with the scalar values $E(t,z)$ and $H(t,z)$. In this case Maxwell's equations become

$$\frac{\partial E}{\partial z} = -\mu_0 \frac{\partial H}{\partial t} \tag{2.5a}$$
$$-\frac{\partial H}{\partial z} = \frac{\partial D}{\partial t} + J_s. \tag{2.5b}$$

We take the partial derivative of Eq. (2.5a) with respect to z, and the partial of Eq. (2.5b) with respect to t. Equating the $\frac{\partial^2 H}{\partial z \partial t}$ terms in each, and thus eliminating the magnetic field H, we have

$$E'' = \mu_0(\ddot{D} + \dot{J}_s),$$

where $'$ denotes z derivatives and $\dot{}$ denotes time derivatives. Using the constitutive law for he electric flux density given by $D = \epsilon_0\epsilon_\infty E + P$, we have

$$\mu_0\epsilon_0\epsilon_\infty \ddot{E} + \mu_0 \ddot{P} - E'' = -\mu_0 \dot{J}_s \text{ in } \Omega = [a,b]. \tag{2.6}$$

In order to have a finite computational domain, we impose absorbing boundary conditions at $z = a$ and $z = b$, which are modeled as

$$[\dot{E} - \mathrm{c}E']_{z=a} = 0, \quad [\dot{E} + \mathrm{c}E']_{z=b} = 0,$$

where $c = 1/\sqrt{\epsilon_0\mu_0}$ is the speed of light in vacuum. With these boundary conditions, any incident signal passes out of the computational domain, and does not return. The homogeneous initial conditions in 1D become

$$E(0,z) = 0, \quad P(0,z) = 0, \quad \dot{P}(0,z) = 0, \quad \dot{E}(0,z) = 0.$$

III. NUMERICAL SOLUTION

We describe in this section the application of finite elements for the spatial discretization of the model (2.6). The semi-discrete model is then coupled with a polarization model, and the system is discretized in time using a theta scheme. The resulting methods are compared in subsequent sections to FDTD methods with respect to stability and dispersion properties.

A. Spatial Discretization Using Finite Elements

We apply a finite element method using standard piecewise linear one dimensional basis elements to discretize the model (2.6) in space. Let N be the number of intervals in the uniform discretization of z, and $\Delta z = (b-a)/N$; then the finite element discretization has an order of accuracy of

$O(\Delta z^2)$. The resulting system of ordinary differential equations after the spatial discretization is the semi-discrete form

$$\epsilon_\infty \mu_0 \epsilon_0 M\ddot{e} + \mu_0 M\ddot{p} + B\dot{e} + Ke = \mu_0 J, \tag{3.1}$$

with either $p \equiv 0$ (Vacuum),

$$\dot{p} + \lambda p = \epsilon_0 \epsilon_d \lambda e, \text{ (Debye Media)}, \tag{3.2}$$

or

$$\ddot{p} + \lambda \dot{p} + \omega_0^2 p = \epsilon_0 \epsilon_d \omega_0^2 e, \text{ (Lorentz Media)}, \tag{3.3}$$

where $\lambda := \frac{1}{\tau}$ (the notation := is used to denote "is defined to be"). The vectors e and p represent the values of E, and P, respectively at the nodes $z_i = i\Delta z, i = 0, 1, \ldots, N$. The mass matrix M has entries

$$M_{ij} = \langle \phi_i, \phi_j \rangle := \int_a^b \phi_i \phi_j dz,$$

where $\{\phi_i\}_{i=0}^N$ are the basis functions. The stability matrix K has entries

$$K_{ij} = \langle \phi_i', \phi_j' \rangle := \int_a^b \phi_i' \phi_j' dz.$$

The matrix B results from the boundary conditions where

$$B_{ij} = \frac{1}{c}[\phi_i(a)\phi_j(a) - \phi_i(b)\phi_j(b)].$$

Finally, J is defined as

$$J_i = -\langle \phi_i, \dot{J}_s \rangle := -\int_a^b \dot{J}_s \phi_i dz.$$

For linear finite elements in one dimension, the entries of the mass matrix M are

$$M_{ij} = \begin{cases} 2\Delta z/3, & \text{if } 0 < i = j < N, \\ \Delta z/3, & \text{else if } i = j = 0 \text{ or } N, \\ \Delta z/6, & \text{else if } i = j \pm 1. \end{cases}$$

The entries of the stiffness matrix can be calculated as

$$K_{ij} = \begin{cases} 2/\Delta z, & \text{if } 0 < i = j < N, \\ 1/\Delta z, & \text{else if } i = j = 0 \text{ or } N, \\ -1/\Delta z, & \text{else if } i = j \pm 1. \end{cases}$$

For Debye media, we differentiate (3.2) and substitute for $\ddot{p}$ into (3.1) to obtain an equation only dependent explicitly on p, given as

$$\epsilon_\infty M\ddot{e} + (B + \epsilon_d \lambda M)\dot{e} + (c^2 K - \epsilon_d \lambda^2 M)e + \frac{\lambda^2}{\epsilon_0} Mp = \frac{1}{\epsilon_0} J, \tag{3.4a}$$

$$\dot{p} + \lambda p - \epsilon_0 \epsilon_d \lambda e = 0. \tag{3.4b}$$

For Lorentz media we substitute (3.3) into (3.1) to obtain

$$\epsilon_\infty M\ddot{e} + B\dot{e} + (c^2K + \epsilon_d\omega_0^2 M)e - \frac{\omega_0^2}{\epsilon_0}Mp - \frac{\lambda}{\epsilon_0}M\dot{p} = \frac{1}{\epsilon_0}J, \tag{3.5a}$$

$$\ddot{p} + \lambda\dot{p} + \omega_0^2 p = \epsilon_0\epsilon_d\omega_0^2 e. \tag{3.5b}$$

B. Time Discretization Using Finite Differences

To solve the semi-discrete form of our equations we may convert each (free space, Debye, Lorentz) coupled second order system of equations into one larger first order system. Thus, we obtain a system of equations of the form

$$\bar{M}\dot{X} + \bar{K}X = \bar{J}, \tag{3.6}$$

for appropriate matrices $\bar{M}$, $\bar{K}$ and $\bar{J}$, and vector X. Applying a theta scheme ([35]) to (3.10) we obtain a system of equations of the form

$$(\bar{M} + \theta\Delta t\bar{K})X^{n+1} = (\bar{M} - (1-\theta)\Delta t\bar{K})X^n + (\theta\bar{J}^{n+1} + (1-\theta)\bar{J}^n). \tag{3.7}$$

For $\theta = 0.5$ the scheme (3.7) can be written as

$$\left(\bar{M} + \frac{\Delta t}{2}\bar{K}\right)X^{n+1} = \left(\bar{M} - \frac{\Delta t}{2}\bar{K}\right)X^n + \frac{1}{2}(\bar{J}^{n+1} + \bar{J}^n) \tag{3.8}$$

where, $\bar{J}^n = \bar{J}(n\Delta t)$ and $X^n = X(n\Delta t)$. As our finite element method is second order in space, if we choose $\theta = \frac{1}{2}$ the discretization is second order in time as well (thus, we have used $\theta = \frac{1}{2}$ throughout). Therefore, for appropriately smooth data and with $\Delta t = O(\Delta z)$, the combined method is second order in time and space.

For the system of equations corresponding to the Debye model we will consider an additional method of temporal finite difference for comparison. However, for completeness, we begin with the simple case of a vacuum.

***Free Space* (FEM-V)** In vacuum we have $\epsilon_\infty = 1$ and $P \equiv 0$. Thus, in Eq. (3.1) we substitute $\ddot{p} = 0$, resulting in

$$\mu_0\epsilon_0 M\ddot{e} + B\dot{e} + Ke = \mu_0 J. \tag{3.9}$$

Rewriting (3.9) in first order form in the variables $X = [e^T,\ d^T]^T$, where $d = \dot{e}$, we have

$$\bar{M}^{\mathrm{V}}\dot{X} + \bar{K}^{\mathrm{V}}X = \bar{J}^{\mathrm{V}}, \tag{3.10}$$

with

$$\bar{M}^{\mathrm{V}} = \begin{bmatrix} I & 0 \\ 0 & \frac{1}{c^2}M \end{bmatrix}, \quad \bar{K}^{\mathrm{V}} = \begin{bmatrix} 0 & -I \\ K & B \end{bmatrix}, \quad \bar{J}^{\mathrm{V}} = \begin{bmatrix} 0 \\ \mu_0 J \end{bmatrix}. \tag{3.11}$$

Using $\bar{M} = \bar{M}^{\mathrm{V}}$, $\bar{K} = \bar{K}^{\mathrm{V}}$ and $\bar{J} = \bar{J}^{\mathrm{V}}$ in (3.8) we obtain the fully discretized finite element method in free space which we denote as **FEM-V**.

Debye Media In the first method to be considered for the Debye model, we will convert the coupled second order system of equations into one larger first order system and apply a theta method as described earlier. In the second method, we will solve first for the polarization with a forward differencing scheme using the initial conditions, and then use the polarization solution vector to update a second order central difference scheme for the magnitude of the electric field. We then continue this process iteratively, alternating between solving for p and for e. Both methods are second order in time and space for appropriately smooth data (and with $\Delta t = O(\Delta z)$).

Method 1 (**FEM-D1**): For Debye media we convert (3.4a)–(3.4b) into a first order system of equations in three unknowns, $X = [e^T, p^T, d^T]^T$, where $d = \dot{e}$, resulting in

$$\bar{M}^{\mathrm{D}}\dot{X} + \bar{K}^{\mathrm{D}}X = \bar{J}^{\mathrm{D}}, \tag{3.12}$$

with

$$\bar{M}^{\mathrm{D}} = \begin{bmatrix} I & 0 & 0 \\ 0 & I & 0 \\ 0 & 0 & \epsilon_\infty M \end{bmatrix}, \quad \bar{K}^{\mathrm{D}} = \begin{bmatrix} 0 & 0 & -I \\ -\epsilon_0\epsilon_d\lambda & \lambda & 0 \\ (c^2K - \epsilon_d\lambda^2 M) & \frac{\lambda^2}{\epsilon_0}M & B + \epsilon_d\lambda M \end{bmatrix}, \tag{3.13}$$

and

$$\bar{J}^{\mathrm{D}} = \begin{bmatrix} 0^T & 0^T & \frac{1}{\epsilon_0}J^T \end{bmatrix}^T. \tag{3.14}$$

We apply a theta-scheme with $\theta = 0.5$ to (3.12) to obtain (3.8) with $\bar{M} = \bar{M}^{\mathrm{D}}, \bar{K} = \bar{K}^{\mathrm{D}}$ and $\bar{J} = \bar{J}^{\mathrm{D}}$. As we are assuming a fixed time step Δt, the matrix to be inverted does not change over time. For a discussion of the solution of the associated linear systems we refer the reader to [36].

Method 2 (**FEM-D2**): In our second method we use a second order central difference scheme to solve (3.4a). Our approach is to first solve for p using a θ-method, and then use that approximation to solve for e at the next time step. Thus, our finite difference approximation for (3.4b) is

$$p^{n+1} = p^n - \Delta t\lambda p^{n+\theta} + \Delta t\lambda\epsilon_d e^{n+\theta}$$

where $v^{n+\theta} = \theta v^{n+1} + (1-\theta)v^n$, for $v = e$ or $v = p$. This implies

$$p^{n+1} = p^n + \frac{\lambda\Delta t}{1 + \lambda\Delta t\theta}(\epsilon_d e^{n+\theta} - p_n). \tag{3.15}$$

Once we have p^{n+1} we can solve for e^{n+2}. Applying second order central difference with averaging to (3.4a) gives

$$\frac{1}{\Delta t^2}\epsilon_\infty M(e^{n+2} - 2e^{n+1} + e^n) + \frac{1}{2\Delta t}(B + \epsilon_d\lambda M)(e^{n+2} - e^n)$$
$$+ \frac{1}{4}(c^2K - \epsilon_d\lambda^2 M)(e^{n+2} + 2e^{n+1} + e^n) = \frac{1}{\epsilon_0}J^{n+1} - \frac{\lambda^2}{\epsilon_0}Mp^{n+1}.$$

Defining $h_\tau = \lambda \Delta t = \frac{\Delta t}{\tau}$ and solving for the e^{n+2} term we have

$$\left[\left(\epsilon_\infty + \frac{\epsilon_d h_\tau}{2} - \frac{\epsilon_d h_\tau^2}{4}\right) M + \frac{1}{2}\Delta t B\right] e^{n+2} = \left[\left(2\epsilon_\infty + \frac{\epsilon_d h_\tau^2}{2}\right) M - \frac{c^2 \Delta t^2}{2} K\right] e^{n+1}$$
$$- \left[\left(\epsilon_\infty - \frac{\epsilon_d h_\tau}{2} - \frac{\epsilon_d h_\tau^2}{4}\right) M + \frac{c^2 \Delta t^2}{4} K + \frac{1}{2}\Delta t B\right] e^n + \frac{\Delta t^2}{\epsilon_0} J^{n+1} - \frac{h_\tau^2}{\epsilon_0} M p^{n+1} \tag{3.16}$$

or equivalently,

$$A_1 e^{n+2} = A_2 e^{n+1} + A_3 e^n + \frac{\Delta t^2}{\epsilon_0} J^{n+1} - \frac{h_\tau^2}{\epsilon_0} M p^{n+1}. \tag{3.17}$$

Again, for $\theta = \frac{1}{2}$, (3.15) will be second order in time if the corresponding solution is C^3 in time. Equation (3.17) is also second order in time assuming an exact solution for P, and that E has four continuous time derivatives (for the second order difference approximation). The truncation error for this approximation is (see [37])

$$T(t_n) = \Delta t^2 \left(\frac{1}{12} E^{(4)} + \frac{1}{6} E^{(3)} + \frac{1}{4} E^{(2)}\right).$$

Therefore, since the semi-discrete form is $O(\Delta z^2)$, this approximation method overall is $O(\Delta z^2)$ when $\Delta t = O(\Delta z)$.

***Lorentz Media* (FEM-L)** For Lorentz media we consider only the approach of converting (3.5a)–(3.5b) into a first order system of equations, which with a theta method for the temporal discretization, we will refer to as the **FEM-L** method. The linear ODE system is in terms of three unknowns, $X = [e^T, p^T, d^T, q^T]^T$, where $d = \dot{e}, q = \dot{p}$, and can be written as

$$\bar{M}^{\mathrm{L}} \dot{X} + \bar{K}^{\mathrm{L}} X = \bar{J}^{\mathrm{L}}, \tag{3.18}$$

with

$$\bar{M}^{\mathrm{L}} = \begin{bmatrix} I & 0 & 0 & 0 \\ 0 & I & 0 & 0 \\ 0 & 0 & \epsilon_\infty M & 0 \\ 0 & 0 & 0 & I \end{bmatrix}, \quad \bar{K}^{\mathrm{L}} = \begin{bmatrix} 0 & 0 & -I & 0 \\ 0 & 0 & 0 & -I \\ (c^2 K + \epsilon_d \omega_0^2 M) & -\frac{\omega_0^2}{\epsilon_0} M & B & -\frac{\lambda}{\epsilon_0} M \\ -\epsilon_0 \epsilon_d \omega_0^2 & \omega_0^2 & 0 & \lambda \end{bmatrix}, \tag{3.19}$$

and

$$\bar{J}^{\mathrm{L}} = \begin{bmatrix} 0^T & 0^T & \frac{1}{\epsilon_0} J^T & 0^T \end{bmatrix}^T. \tag{3.20}$$

Again, we apply a theta-scheme with $\theta = 0.5$ to (3.18) to obtain (3.8) with $\bar{M} = \bar{M}^{\mathrm{L}}$, $\bar{K} = \bar{K}^{\mathrm{L}}$ and $\bar{J} = \bar{J}^{\mathrm{L}}$.

IV. STABILITY ANALYSIS

Fourier analysis is an important tool in the study of stability of finite difference and finite element schemes. The Fourier transform of a function gives an alternative representation of the function, and one can infer certain properties of a function from its Fourier transform. The Fourier inversion formula represents a function as a superposition of waves $e^{i\omega z}$ with different amplitudes that are given by the Fourier transform. Under the Fourier transform the operation of differentiation is converted into the operation of multiplication by $i\omega$.

An important application of Fourier analysis is the von Neumann analysis of stability of difference schemes. With the use of Fourier analysis we can give necessary and sufficient conditions for the stability of these schemes. For a difference scheme, advancing the solution of the scheme by one time step is equivalent to multiplying the Fourier transform of the solution by an *amplification factor*. The amplification factor is so called because its magnitude is the amount that the amplitude of each frequency in the solution, given by the Fourier transform of the solution at time step n, is amplified in advancing the solution to time step $n + 1$. All the information of a scheme is contained in its amplification factor. In particular, the stability and accuracy of schemes can be determined from the amplification factor. Using Fourier analysis on the scheme to calculate the amplification factor ζ is equivalent to replacing discrete values of any unknown field vector v_m^n, at time $t = n\Delta t$ and spatial position $z = m\Delta z$, in the scheme by $\zeta^n e^{im\theta}$ for each value of n and m. The resulting equation is a polynomial in ζ and is called the *stability polynomial* or the *characteristic polynomial* for the scheme. The stability polynomial usually depends on the discretization parameters, such as the time step and the mesh step size as well as the medium parameters. The roots of this polynomial can be obtained and will determine the stability of the scheme. Since the roots of the polynomial are the amplification factors of the scheme, the scheme will be stable if the amplitude of the roots is less than or equal to 1.

We follow here the approach used in [7] for the FDTD method in order to derive stability results for the finite element schemes described earlier. We will compare our results with those obtained in [7] for FDTD schemes treating both Debye and Lorentz models. Namely, for Debye, we consider the scheme in [12] (which we will refer to as JHT-D) and the scheme in [13] (KF-D). Regarding the Lorentz model for polarization, we compare results with JHT-L [12] and KF-L [14].

Note that, since the boundary conditions do not affect the stability and dispersion properties of the scheme in the interior of the domain, we neglect the effects of boundary conditions, i.e., we take $B = 0$ in (3.1), in our analysis. Further, as the stability and dispersion properties of the scheme are also independent of the source J_s, we take $J = 0$ in (3.1) without loss of generality.

A. Free Space

We note the following identities associated with the application of the mass and the stiffness matrices on vectors $\phi_j^n = \tilde{\phi}\zeta^n e^{i(kj\Delta z)}$

1. For the mass matrix M we have

$$M\phi_j^n = (3 - 2\sin^2(k\Delta z/2))\frac{\Delta z}{3}\phi_j^n \tag{4.1}$$

2. For the stiffness matrix K we have

$$K\phi_j^n = \frac{4}{\Delta z}\sin^2(k\Delta z/2))\phi_j^n. \tag{4.2}$$

We also define two quantities

$$\kappa = 3 - 2\sin^2\left(\frac{k\Delta z}{2}\right), \tag{4.3a}$$

$$\eta = 3\nu^2 \sin^2\left(\frac{k\Delta z}{2}\right), \tag{4.3b}$$

where the *Courant number* for a general dispersive material is $\nu = \frac{c\Delta t}{\sqrt{\epsilon_\infty}\Delta z}$. In free space $\epsilon_\infty = 1$. To determine the stability criterion for the finite element scheme in vacuum, FEM-V, we now substitute

$$X_j^n = \begin{bmatrix} e_j^n \\ d_j^n \end{bmatrix} = \begin{bmatrix} \tilde{e} \\ \tilde{d} \end{bmatrix} \zeta^n \mathrm{e}^{\mathrm{i}(kj\Delta z)},$$

into the discrete Eq. (3.8) with $\bar{M} = \bar{M}^{\mathrm{V}}, \bar{K} = \bar{K}^{\mathrm{V}}$ and $\bar{J} = \bar{J}^{\mathrm{V}}$ as given in (3.11) (with $B \equiv 0, J \equiv 0$). Here k is the wave number, Using the identities (4.1) and (4.2) we obtain a homogeneous linear system of the form $\mathcal{A}\tilde{\mathcal{X}} = 0$. By setting the determinant of $\mathcal{A}$ to zero we obtain the stability polynomial

$$\zeta^2 - 2\zeta\left(\frac{\kappa^2 - \eta^2}{\kappa^2 + \eta^2}\right) + 1 = 0, \tag{4.4}$$

From (4.4) we can show that $|\zeta| = 1$ always, regardless of the medium parameters. This implies that the finite element scheme with the theta method ($\theta = 1/2$) in *free space*, FEM-V, is *unconditionally stable* as well as *non-dissipative*.

B. Debye Media

To determine the stability conditions for the finite element scheme FEM-D1 described in "Debye Media" section we substitute

$$X_j^n = \begin{bmatrix} e_j^n \\ p_j^n \\ d_j^n \end{bmatrix} = \begin{bmatrix} \tilde{e} \\ \tilde{p} \\ \tilde{d} \end{bmatrix} \zeta^n \mathrm{e}^{\mathrm{i}kj\Delta z}, \tag{4.5}$$

in the discrete Eq. (3.8) with $\bar{M} = \bar{M}^{\mathrm{D}}, \bar{K} = \bar{K}^{\mathrm{D}}$ and $\bar{J} = \bar{J}^{\mathrm{D}}$ as given in (3.13)–(3.14) (with $B \equiv 0, J \equiv 0$).

As in the case of free space, we obtain a homogeneous system of the type $\mathcal{A}\tilde{\mathcal{X}} = 0$. We then set $\det(\mathcal{A}) = 0$ to obtain the stability polynomial

$$a_3\zeta^3 + a_2\zeta^2 + a_1\zeta + a_0 = 0, \tag{4.6}$$

where the coefficients of the stability polynomial are given by

$$a_3 = \eta^2(h_\tau + 2) + \kappa^2(h_\tau\epsilon_s + 2\epsilon_\infty), \tag{4.7}$$

$$a_2 = \eta^2(3h_\tau + 2) - \kappa^2(h_\tau\epsilon_s + 6\epsilon_\infty), \tag{4.8}$$

$$a_1 = \eta^2(3h_\tau - 2) - \kappa^2(h_\tau\epsilon_s - 6\epsilon_\infty), \tag{4.9}$$

$$a_0 = \eta^2(h_\tau - 2) + \kappa^2(h_\tau\epsilon_s - 2\epsilon_\infty), \tag{4.10}$$

with η, and κ are as defined in (4.3b), and (4.3a), respectively, and as before $h_\tau = \lambda \Delta t = \frac{\Delta t}{\tau}$.

To determine the stability polynomial for the finite element scheme FEM-D2 described in "Debye Media" section, we substitute (4.5) in the discrete Eq. (3.16) (with $B \equiv 0, J \equiv 0$). Following the procedure discussed earlier we obtain the stability polynomial

$$b_3\zeta^3 + b_2\zeta^2 + b_1\zeta + b_0 = 0, \tag{4.11}$$

with coefficients

$$b_3 = \eta^2(h_\tau + 2) + \kappa^2(h_\tau\epsilon_s + 2\epsilon_\infty) - \frac{\kappa^2 h_\tau^3 \epsilon_d}{4}, \tag{4.12}$$

$$b_2 = \eta^2(3h_\tau + 2) - \kappa^2(h_\tau\epsilon_s + 6\epsilon_\infty) + \frac{\kappa^2 h_\tau^3 \epsilon_d}{4}, \tag{4.13}$$

$$b_1 = \eta^2(3h_\tau - 2) - \kappa^2(h_\tau\epsilon_s - 6\epsilon_\infty) + \frac{\kappa^2 h_\tau^3 \epsilon_d}{4}, \tag{4.14}$$

$$b_0 = \eta^2(h_\tau - 2) + \kappa^2(h_\tau\epsilon_s - 2\epsilon_\infty) - \frac{\kappa^2 h_\tau^3 \epsilon_d}{4}. \tag{4.15}$$

In [36] a plot of $\max|\zeta|$ versus $k\Delta z$ is given for $h_\tau = 0.1$ and $h_\tau = 0.3$ for the finite element schemes FEM-D1 and FEM-D2, with $\nu = 1$. From this plot one can see a slight difference in the two schemes when $h_\tau = 0.3$. However, for $h_\tau = 0.1$ the two schemes are indistinguishable. Therefore, in the rest of this section we will consider only FEM-D1, and may refer to it as *the finite element scheme* for the Debye model. Similarly, it was shown in [7] that the stability properties for the two FDTD methods JHT-D [12] and KF-D [13] are identical. Therefore, in the remainder of this section we will consider only JHT-D, and may refer to it as *the finite difference scheme* for the Debye model. We will compare stability properties of the finite element scheme FEM-D1 with those of the finite difference scheme JHT-D, understanding that the corresponding conclusions drawn therein apply equally to the methods FEM-D2 and KF-D.

In the left plot of Fig. 1 we graph the absolute value of the largest root of (4.6), as a function of $k\Delta z$, for the finite element scheme FEM-D1 using $\nu = 1$. We can interpret $k\Delta z$ as the wave number if Δz is fixed, or as the inverse of the number of points per wavelength (N_{ppw}) if k is fixed. In Fig. 2 we plot the absolute value of the largest root of the stability polynomial of the finite difference scheme JHT [12], with $\nu = 1$ as a function of $k\Delta z$. In each figure, the right plot depicts the same quantity, but versus the wave number k.

To generate these plots we assumed the following values of the physical parameters, as considered in [25] (note that these are appropriate constants for modeling water)

$$\epsilon_\infty = 1, \quad \epsilon_s = 78.2, \quad \tau = 8.1 \times 10^{-12} \text{ sec}. \tag{4.16}$$

The time step Δt is determined by the choice of h_τ and the physical parameter τ. These plots show varying values of h_τ from 0.1 to 0.001. From the plots we can see that the dissipation of the numerical schemes can be reduced by decreasing h_τ. For stability and least dissipation, $h_\tau = 0.001$ is recommended, which is in agreement with the guideline for FDTD. For the finite element scheme FEM-D1, increasing ν from 1 to 16 does not appear to change the stability behavior of the scheme. This suggests the *unconditional stability* of *the finite element scheme* for Debye media. However, *the finite difference scheme is conditionally stable* and has the stability criteria $\nu \leq 1$. The stability criteria for the finite difference schemes have been derived in [7, 23].

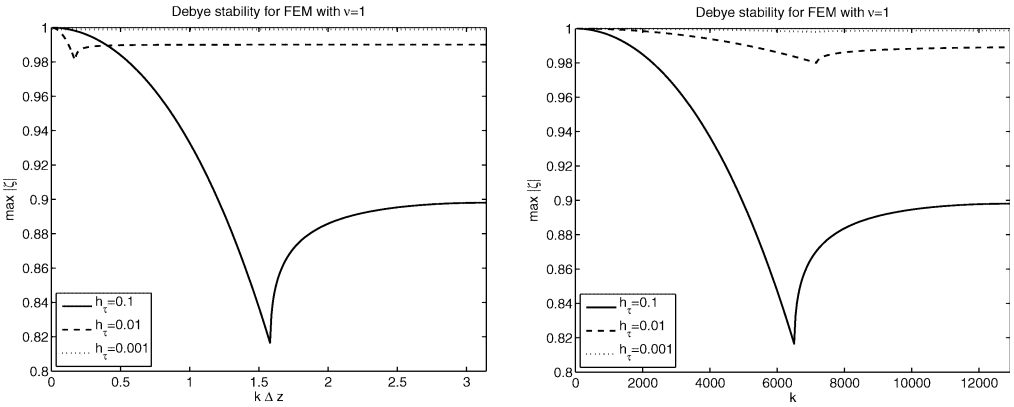

FIG. 1. Plot on left (right) is of $\max|\zeta|$ versus $k\Delta z$ (resp., k) for $h_\tau \in \{0.1, 0.01, 0.001\}$ for the FEM-D1 scheme, with $\nu = 1$.

C. Lorentz Media

To determine the stability conditions for the finite element method applied to the Lorentz media, FEM-L, we substitute

$$X_j^n = \begin{bmatrix} e_j^n \\ p_j^n \\ d_j^n \\ q_j^n \end{bmatrix} = \begin{bmatrix} \tilde{e} \\ \tilde{p} \\ \tilde{d} \\ \tilde{q} \end{bmatrix} \zeta^n \mathrm{e}^{\mathrm{i}kj\Delta z},$$

in the discrete Eq. (3.8) with $\bar{M} = \bar{M}^{\mathrm{L}}$, $\bar{K} = \bar{K}^{\mathrm{L}}$ and $\bar{J} = \bar{J}^{\mathrm{L}}$ as given in (3.19)–(3.20) (with $B \equiv 0, J \equiv 0$).

As in the case of free space, we obtain a homogeneous system of the type $\mathcal{A}\tilde{\mathcal{X}} = 0$. We then set $\det(\mathcal{A}) = 0$ to obtain the stability polynomial

$$a_4\zeta^4 + a_3\zeta^3 + a_2\zeta^2 + a_1\zeta + a_0 = 0, \tag{4.17}$$

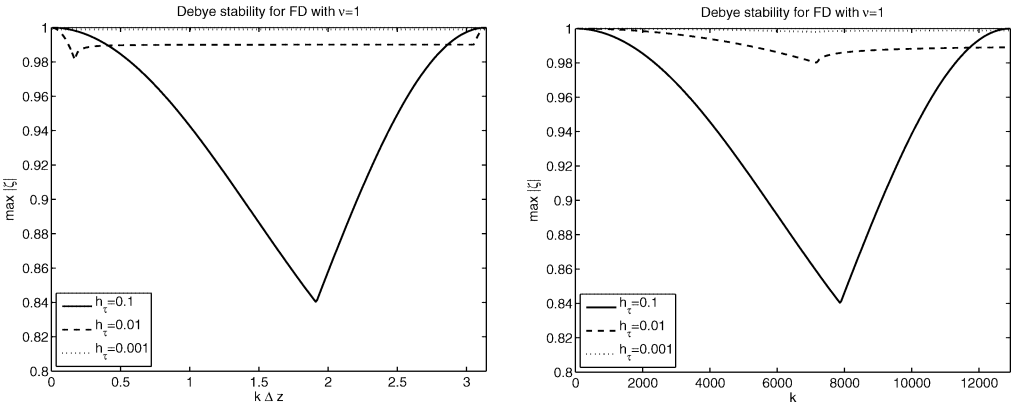

FIG. 2. Plot on left (right) is of $\max|\zeta|$ versus $k\Delta z$ (resp., k) for $h_\tau \in \{0.1, 0.01, 0.001\}$ for the JHT-D scheme, with $\nu = 1$.

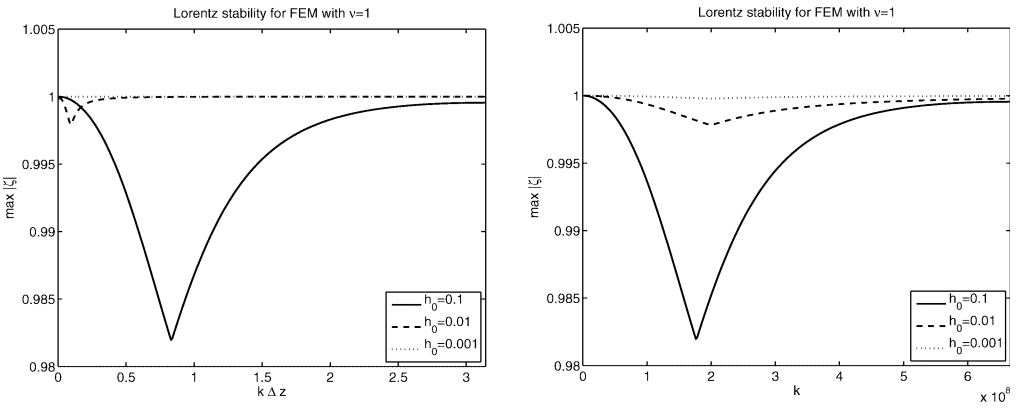

FIG. 3. Plot on left (right) is of $\max|\zeta|$ versus $k\Delta z$ (resp., k) for $h_\tau \in \{0.1, 0.01, 0.001\}$ for the FEM-L scheme, with $\nu = 1$.

where the coefficients of the stability polynomial are given by

$$a_4 = \eta^2\big(2\pi^2 h_0^2 + h_\tau + 2\big) + \kappa^2\big(2\pi^2 h_0^2 \epsilon_s + h_\tau \epsilon_\infty + 2\epsilon_\infty\big) \tag{4.18}$$

$$a_3 = \eta^2\big(8\pi^2 h_0^2 + 2h_\tau\big) - \kappa^2 \epsilon_\infty (8 + 2h_\tau) \tag{4.19}$$

$$a_2 = \eta^2\big(12\pi^2 h_0^2 - 4\big) - \kappa^2\big(4\pi^2 h_0^2 \epsilon_s - 12\epsilon_\infty\big) \tag{4.20}$$

$$a_1 = \eta^2\big(8\pi^2 h_0^2 - 2h_\tau\big) - \kappa^2 \epsilon_\infty (8 - 2h_\tau) \tag{4.21}$$

$$a_0 = \eta^2\big(2\pi^2 h_0^2 - h_\tau + 2\big) - \kappa^2\big(2\pi^2 h_0^2 \epsilon_s - h_\tau \epsilon_\infty + 2\epsilon_\infty\big), \tag{4.22}$$

with η, and κ as defined in (4.3b), and (4.3a), respectively, $h_\tau = \Delta t/\tau$, and $h_0 = \Delta t/T_0$, with $T_0 = 2\pi/\omega_0$.

We seek to compare the stability properties of FEM-L to the finite difference schemes JHT-L [12] and KF-L [14]. We plot the absolute value of the largest root of (4.17) for $\nu = 1$ versus $k\Delta z$ for the FEM-L in Fig. 3 (left), and for the schemes JHT-L and KF-L, we plot the corresponding functions on the left in Figs. 4 and 5, respectively. In each figure, the right plot depicts the same function as the left plot, but versus the wave number k.

To generate these plots we assumed the following values for physical parameters, as considered in [7]:

$$\epsilon_\infty = 1, \quad \epsilon_s = 2.25, \quad \tau = 1.786 \times 10^{-16} \text{ sec}, \quad \omega_0 = 4 \times 10^{16} \text{ rad/sec}. \tag{4.23}$$

These are typical values that are used in the study of physical optics and are representative of a highly absorptive and dispersive medium [38]. These values will also be used in our numerical examples involving the Lorentz polarization model.

For the Lorentz medium, all time scales must be properly resolved, therefore the time step Δt is determined by the choice of either h_τ or h_0, whichever is most restrictive. For the current parameter values, $T_0 < \tau$, thus h_0 is used. The plots show varying values of h_0 from 0.1 to 0.001. From the plots we can see that the dissipation of the numerical schemes can be reduced by decreasing h_0. For stability and least dissipation, $h_0 = 0.01$ is recommended, which again is in agreement with the guideline for the FDTD scheme.

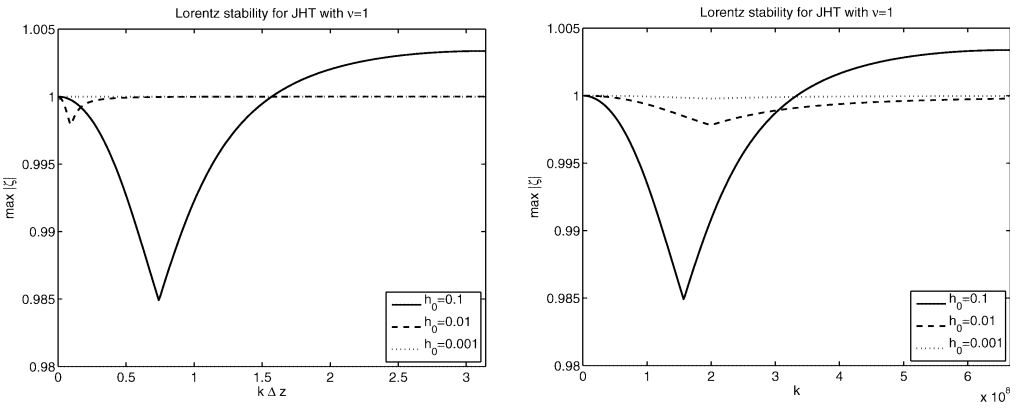

FIG. 4. Plot on left (right) is of $\max|\zeta|$ versus $k\Delta z$ (resp., k) for $h_\tau \in \{0.1, 0.01, 0.001\}$ for the JHT-L scheme, with $\nu = 1$.

As in the case of the finite element method for Debye media, FEM-D1, we see that increasing ν from 1 to 16 does not affect the stability properties of the finite element scheme for Lorentz media, FEM-L (see [36] for details). This suggests the *unconditional stability* of the *finite element method* for Lorentz media. However, again *the finite difference scheme is conditionally stable* with the criteria $\nu \leq 1$. The stability criteria for the finite difference scheme for Lorentz media have been derived in [7, 23].

V. ANALYSIS OF DISPERSION AND PHASE ERROR

The numerical models presented admit plane wave solutions of the form $e^{i(\omega t - \vec{k}\cdot\vec{x})}$ for which the speed of propagation, governed by the wave number $\vec{k}$, erroneously depends on the frequency ω. The resulting error in the solution, which is an artifact of discretization, is termed as numerical dispersion. For time-harmonic waves, numerical dispersion results in the creation of a numerical

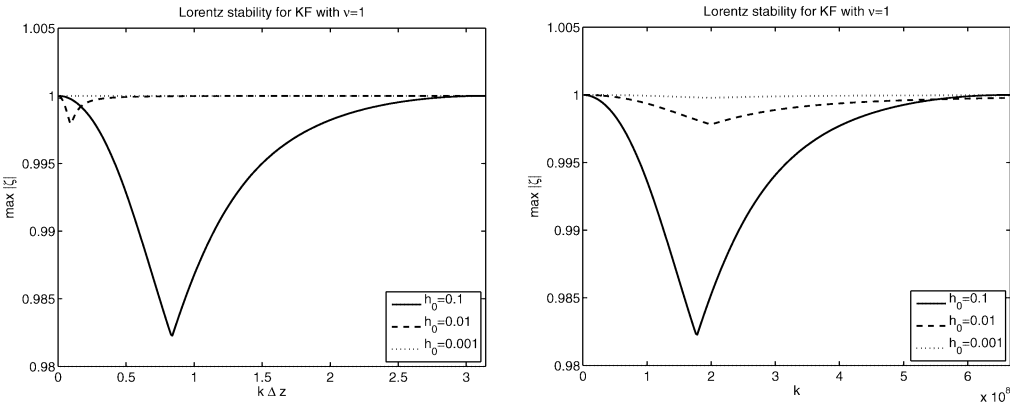

FIG. 5. Plot on left (right) is of $\max|\zeta|$ versus $k\Delta z$ (resp., k) for $h_\tau \in \{0.1, 0.01, 0.001\}$ for the KF-L scheme, with $\nu = 1$.

phase velocity error, or *phase error*, in the solution. This is due to the incorrect modeling of the sinusoidal behavior of the propagating wave; for example, the piecewise polynomial approximation of a finite element method does not exactly match a sine or cosine function. Dispersion is present in numerical approximation methods such as finite difference/finite element methods even in the absence of any physical dispersion in the actual media. As waves propagate over long distances numerical dispersion errors accumulate in the solution and may cause it to completely deviate from the correct solution.

A. Free Space

Substituting a solution of the form

$$e(t,z) = \mathrm{e}^{\mathrm{i}(kz-\omega t)}$$

into Eq. (2.6), we obtain the dispersion relation of the continuous model in free space given by

$$k_{\mathrm{EX}}^{\mathrm{V}}(\omega) = \frac{\omega}{\mathrm{c}},$$

where $k_{\mathrm{EX}}^{\mathrm{V}}$ denotes the wavenumber in free space (where V in the superscript denotes "vacuum") for the exact equations (EX in the subscript denotes "exact"). To determine the dispersion relation for the discretized model using the finite element method FEM-V, we substitute

$$X_j^n = \begin{bmatrix} e_j^n \\ d_j^n \end{bmatrix} = \begin{bmatrix} \tilde{e} \\ \tilde{d} \end{bmatrix} \mathrm{e}^{\mathrm{i}(k_\Delta j\Delta z-\omega n\Delta t)},$$

where k_Δ is the numerical wave number, into the discrete Eq. (3.8) with $\bar{M} = \bar{M}^{\mathrm{V}}$, $\bar{K} = \bar{K}^{\mathrm{V}}$ and $\bar{J} = \bar{J}^{\mathrm{V}}$ as given in (3.11) (with $B \equiv 0$ and $J \equiv 0$). Using the identities (4.1), (4.2) as well as the following two trigonometric identities

$$\mathrm{e}^{-\mathrm{i}\omega\Delta t/2} + \mathrm{e}^{\mathrm{i}\omega\Delta t/2} = 2\cos(\omega\Delta t/2), \tag{5.1a}$$

$$\mathrm{e}^{-\mathrm{i}\omega\Delta t/2} - \mathrm{e}^{\mathrm{i}\omega\Delta t/2} = -2\mathrm{i}\sin(\omega\Delta t/2). \tag{5.1b}$$

We obtain a homogeneous system of the type $\mathcal{A}\tilde{\mathcal{X}} = 0$. We then set $\det(\mathcal{A}) = 0$ to determine a relation between k_Δ and ω, which is the numerical dispersion relation for the finite element scheme in free space, FEM-V. This relation is

$$\sin^2(k_\Delta\Delta z/2) = \left(\frac{2}{3} + \frac{\nu^2\cos^2(\omega\Delta t/2)}{\sin^2(\omega\Delta t/2)}\right)^{-1}. \tag{5.2}$$

Solving for k_Δ in the above we obtain

$$k_\Delta = k_{\mathrm{FE}}^{\mathrm{V}}(\omega) = \frac{2}{\Delta z}\sin^{-1}\left(\left(\frac{2}{3} + \frac{\nu^2\cos^2(\omega\Delta t/2)}{\sin^2(\omega\Delta t/2)}\right)^{-1/2}\right). \tag{5.3}$$

The dispersion relation for the FDTD scheme [39] is given to be

$$\sin(k_\Delta\Delta z/2) = \frac{\sin(\omega\Delta t/2)}{\nu}, \tag{5.4}$$

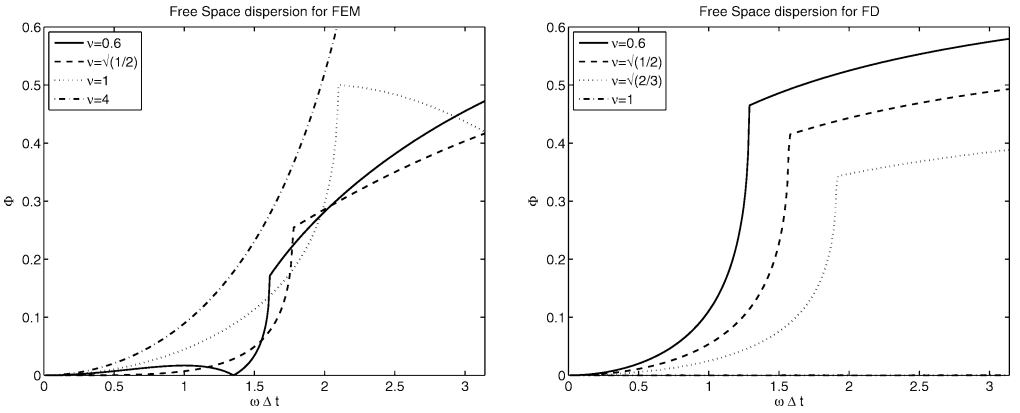

FIG. 6. Plot of the phase error Φ versus $\omega\Delta t$ for FEM-V with $\nu \in \{0.6, \sqrt{1/2}, 1, 4\}$ (left), and FDTD in freespace with $\nu = \{0.6, \sqrt{1/2}, \sqrt{2/3}, 1\}$ (right). For $\nu = 1$ FDTD has zero dispersion.

which implies that

$$k_\Delta = k_{\mathrm{FD}}^{\mathrm{V}}(\omega) = \frac{2}{\Delta z} \sin^{-1}\left[\frac{\sin(\omega\Delta t/2)}{\nu}\right]. \tag{5.5}$$

We will define the phase error for a given method as

$$\Phi(\omega\Delta t) = \left|\frac{k_{\mathrm{EX}}(\omega\Delta t) - k_\Delta(\omega\Delta t)}{k_{\mathrm{EX}}(\omega\Delta t)}\right|, \tag{5.6}$$

where for FEM-V we have $k_\Delta = k_{\mathrm{FE}}^{\mathrm{V}}$ as defined in (5.3), and for the FDTD scheme we have $k_\Delta = k_{\mathrm{FD}}^{\mathrm{V}}$ as defined in (5.5).

In Fig. 6 we plot the phase error in a vacuum for the FEM-V scheme with the theta method using $\nu \in \{0.6, \sqrt{1/2}, 1, 4\}$ (left) and for the FDTD scheme using $\nu \in \{0.6, \sqrt{1/2}, \sqrt{2/3}, 1\}$ (right). We note that for the finite element method, no significant differences were noticed for ν values larger than 4. Thus, in this article we limit ourselves to $\nu \in (0, 4]$ (see [36]).

To see why $\nu = \sqrt{1/2}$ has the least dispersion for FEM-V and why $\nu = 1$ has the least dispersion for the FDTD scheme, it is helpful to plot the relations in Eqs. (5.2) and (5.4) versus the continuous model values. We define

$$\gamma_{\mathrm{EX}}^2 := \sin^2\left(\frac{k_{\mathrm{EX}}^{\mathrm{V}}\Delta z}{2}\right) = \sin^2\left(\frac{\omega\Delta t}{2\nu}\right)$$

where we have substituted $\nu k_{\mathrm{EX}}^{\mathrm{V}}\Delta z = \omega\Delta t$. We similarly define $\gamma_{\mathrm{FE}}^2 = \sin^2(k_{\mathrm{FE}}^{\mathrm{V}}\Delta z/2)$ and $\gamma_{FD}^2 = \sin^2(k_{\mathrm{FD}}^{\mathrm{V}}\Delta z/2)$ using the definitions in (5.3) and (5.5), respectively. Figure 7 displays plots for each of these $\gamma^2(\omega\Delta t)$ functions for various values of ν. For the continuous model (left plot), ν has the effect of moving the location of the maximum value, $\gamma^2 = 1$. For the finite difference case (right plot) the location of the maximum does not change, although the value of the maximum does. For $\nu = 1$ the curve coincides exactly with the continuous case. For the finite element method (middle plot) the location of the maximum does not change, nor does the value. However, as this value is fixed at 1.5, it will *never* coincide exactly with the continuous case for any value of ν.

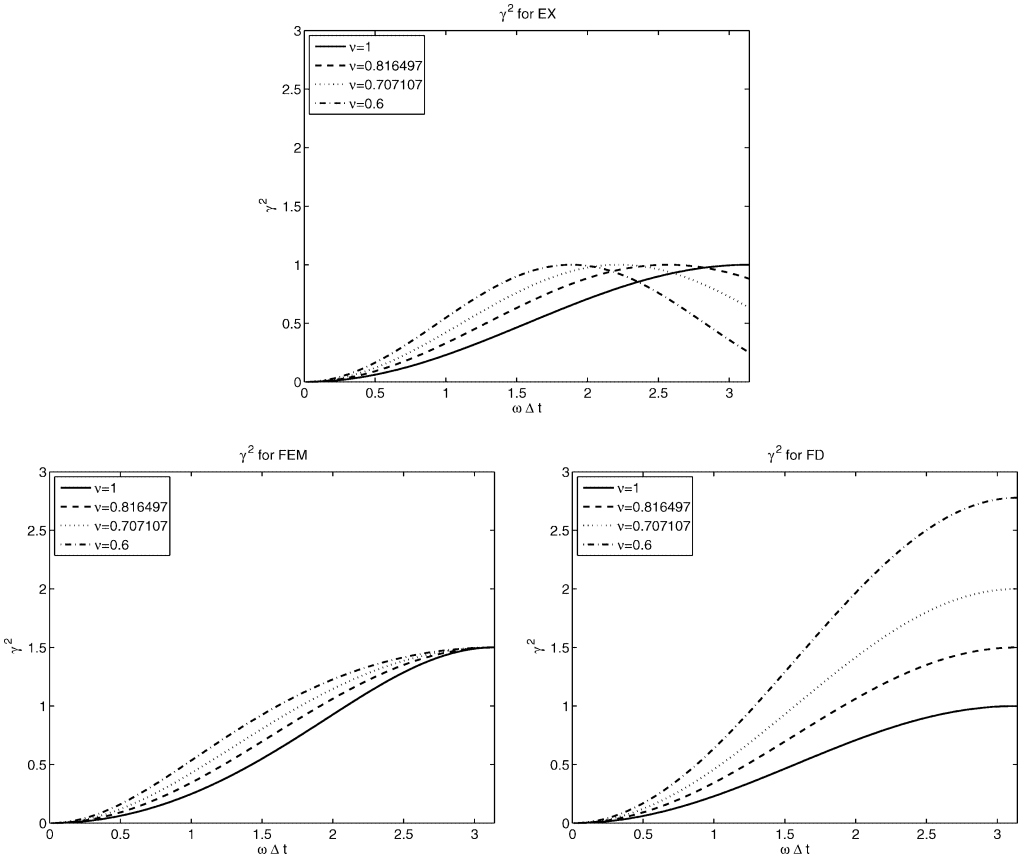

FIG. 7. Plot of the γ^2 versus $\omega\Delta t$ for the continuous model, the finite elment scheme, and the finite difference scheme (left to right).

To determine the *best* value of ν for the finite element method, we first note that γ^2_{EX} can be expanded as

$$\frac{1}{4\nu^2}(\omega\Delta t)^2 - \frac{1}{48\nu^4}(\omega\Delta t)^4 + \frac{1}{1440\nu^6}(\omega\Delta t)^6 + O((\omega\Delta t)^8).$$

As both the expansions of γ_{FD} and γ_{FE} match up to the second order coefficient, it is the Taylor coefficient of $(\omega\Delta t)^4$, i.e.,

$$c_4^{\mathrm{EX}} = -\frac{1}{48\nu^4},$$

that determines how well the discretization method matches the continuous model. For the finite difference method we have

$$c_4^{\mathrm{FD}} = -\frac{1}{48\nu^{-2}},$$

whereas for the finite element method we have

$$c_4^{\mathrm{FE}} = \frac{-1+\nu^2}{24\nu^4}.$$

For $\nu = 1$, $c_4^{\mathrm{FD}} = c_4^{\mathrm{EX}} = -1/48$, but $c_4^{\mathrm{FE}} = 0$. If we solve $(c_4^{\mathrm{EX}} - c_4^{\mathrm{FE}})(\nu) = 0$ we find that $\nu = \sqrt{1/2}$ is the value for which the finite element method most closely matches the continuous model wave number. It can be shown that for $\nu = \sqrt{2/3}$ the FEM-V scheme and the FDTD scheme have almost identical dispersion curves. Further, for $\nu = \sqrt{1/2}$, FEM-V has phase velocity (propagation speed scaled by $\frac{1}{\mathrm{c}}$) closest to one (see [36]). For $\nu = 1$ FDTD always has phase velocity equal to one.

B. Debye Media

The dispersion relation for the continuous Debye model (with $\epsilon_\infty = 1$) is given by

$$k_{\mathrm{EX}}^{\mathrm{D}}(\omega) = \frac{\omega}{\mathrm{c}}\sqrt{\epsilon_r^{\mathrm{D}}(\omega)}, \tag{5.7}$$

where

$$\epsilon_r^{\mathrm{D}}(\omega) := \frac{\epsilon_s\lambda - \mathrm{i}\omega}{\lambda - \mathrm{i}\omega}, \tag{5.8}$$

is the relative complex permittivity of the Debye medium, and $\lambda = 1/\tau$.

We will show below that the numerical dispersion relations for the finite element method as well as the FDTD method can be written in the form

$$k_\Delta^{\mathrm{D}}(\omega) = \frac{2}{\Delta z}\sin^{-1}\left[\frac{\omega_\Delta}{c}\frac{\Delta z}{2}\sqrt{\epsilon_{r,\Delta}^{\mathrm{D}}}\right], \tag{5.9}$$

with the discrete relative complex permittivity given in the form

$$\epsilon_{r,\Delta}^{\mathrm{D}} := \frac{\epsilon_{s,\Delta}\lambda_\Delta - \mathrm{i}\omega_\Delta}{\lambda_\Delta - \mathrm{i}\omega_\Delta}. \tag{5.10}$$

To derive the numerical dispersion relation for the finite element method FEM-D1, described in "Debye Media" section, we substitute

$$X_j^n = \begin{bmatrix} e_j^n \\ p_j^n \\ d_j^n \end{bmatrix} = \begin{bmatrix} \tilde{e} \\ \tilde{p} \\ \tilde{d} \end{bmatrix} \mathrm{e}^{\mathrm{i}(k_\Delta j\Delta z - \omega n\Delta t)}$$

in the discrete Eq. (3.8) with $\bar{M} = \bar{M}^{\mathrm{D}}$, $\bar{K} = \bar{K}^{\mathrm{D}}$ and $\bar{J} = \bar{J}^{\mathrm{D}}$ as given in (3.13)-(3.14) (with $B \equiv 0, J \equiv 0$). We assume again that $\epsilon_\infty = 1$. As in the case of free space, we obtain a homogeneous system of the type $\mathcal{A}\tilde{\mathcal{X}} = 0$. We then set $\det(\mathcal{A}) = 0$ to obtain a relation between the numerical wavenumber k_Δ and the frequency ω. Solving for k_Δ in this relation we obtain the numerical dispersion relation for the FEM-D1 scheme in the form (5.9) with $k_\Delta^{\mathrm{D}}(\omega) = k_{\mathrm{FE}}^{\mathrm{D}}(\omega)$,

the discrete relative complex permittivity in (5.10) with $\epsilon^{\mathrm{D}}_{r,\Delta} = \epsilon^{\mathrm{D}}_{r,\mathrm{FE}}$ and the discrete medium parameters given by

$$\epsilon_{s,\Delta} = \epsilon^{\mathrm{D}}_{s,\mathrm{FE}} := \frac{\epsilon_s}{\alpha^2\beta^2}, \tag{5.11}$$

$$\lambda_\Delta = \lambda^{\mathrm{D}}_{\mathrm{FE}} := \lambda\cos(\omega\Delta t/2)\beta^2\alpha^3, \tag{5.12}$$

$$\omega_\Delta = \omega^{\mathrm{D}}_{\mathrm{FE}} := \omega s_\omega \alpha, \tag{5.13}$$

where in the above we have used the following simplifying variables:

$$s_\omega = \frac{\sin(\omega\Delta t/2)}{\omega\Delta t/2}, \tag{5.14}$$

$$\alpha = \left(\frac{2\sin^2(\omega\Delta t/2)}{3\nu^2} + \cos^2(\omega\Delta t/2)\right)^{-1/2}, \tag{5.15}$$

$$\beta = \left(\frac{2\epsilon_s\sin^2(\omega\Delta t/2)}{3\nu^2} + \cos^2(\omega\Delta t/2)\right)^{1/2}. \tag{5.16}$$

To determine the numerical dispersion relation for the finite element scheme FEM-D2, described in "Debye Media" section, we substitute (5.2) in the discrete Eq. (3.16). Following the procedure discussed above we obtain the numerical dispersion relation for the FEM-D2 scheme to be

$$\sin^2(k^D_{\mathrm{FE2}}\Delta z/2) = \alpha^2\left(\frac{2\sin(\eta)\mathrm{i} - \lambda\cos(\eta)\epsilon_s\Delta t + \frac{1}{4}h_\tau^3\cos(\eta)\epsilon_d}{2\sin(\eta)\mathrm{i} - \lambda\cos(\eta)\epsilon_s\Delta t\beta^2\alpha^2 + \frac{1}{6}h_\tau^3\cos(\eta)\epsilon_d\alpha^2}\right), \tag{5.17}$$

where $\eta = \frac{\omega\Delta t}{2}$, $\epsilon_d = \epsilon_s - 1$, and $h_\tau = \Delta t/\tau$. If we neglect terms in h_τ^3, then the expression (5.17) reduces to (5.8)–(5.9), with the medium parameters as defined earlier. Thus, for small h_τ, both the finite element methods, FEM-D1 and FEM-D2 have the same numerical dispersion relations. From the section on stability analysis we have seen that for low dissipation h_τ needs to be about 0.001 for Debye media and 0.01 for Lorentz media. For these values of h_τ both finite element schemes produce the same dispersion graphs (see [36]). Therefore, in the rest of this section we will consider only FEM-D1, and may refer to it as *the finite element scheme* for the Debye model. Similarly, it was shown in [7] that the phase error properties for the two FDTD methods JHT-D [12] and KF-D [13] are identical. Therefore, in the remainder of this section we will consider only JHT-D, and may refer to it as *the finite difference scheme* for the Debye model. We will compare dispersion properties of the finite element scheme FEM-D1 with those of the finite difference scheme JHT-D.

The FEM-D1 scheme misrepresents the continuous model parameters λ and ϵ_s discretely as $\lambda^{\mathrm{D}}_{\mathrm{FE}}$ and $\epsilon^{\mathrm{D}}_{s,\mathrm{FE}}$, and misrepresents the frequency ω as $\omega^{\mathrm{D}}_{\mathrm{FE}}$. We note that as ν increases ($\nu > \sqrt{\epsilon_s}$),the product $\alpha\beta \to 1$ thus $\epsilon^D_{s,\mathrm{FE}} \to \epsilon_s$. The discrete parameter $\lambda^{\mathrm{D}}_{\mathrm{FE}}$ is a function of the continuous model parameter ϵ_s via the quantity β. However, for the regime of interest, namely $\omega\Delta t$ small, when ν is large ($\nu > \sqrt{\epsilon_s}$), the quantity $2\epsilon_s\sin^2(\omega\Delta t/2)/3\nu^2$ is dominated by $\cos^2(\omega\Delta t/2)$. Also note that the product $\alpha\beta \to 1$ as $\alpha \to 1/\cos(\omega\Delta/2)$ and thus $\lambda_\Delta \to \lambda$. Finally for $\omega\Delta t$ small and ν large, $s_\omega\alpha \approx 1$ and thus $\omega^{\mathrm{D}}_{\mathrm{FE}} \to \omega$. Hence, the choice of the Courant number ν is important for maintaining low dispersion error in the FEM schemes.

We compare the FEM-D1 scheme for Debye media with the finite difference scheme JHT-D presented in [12] and analyzed in [7]. The numerical dispersion relation for this finite difference scheme can be written in the form of (5.9)–(5.10) where the discrete representations of the continuous model parameters are given as

$$\epsilon_{s,\Delta} = \epsilon^{\mathrm{D}}_{s,\mathrm{FD}} := \epsilon_s \tag{5.18}$$

$$\lambda_{\Delta} = \lambda^{\mathrm{D}}_{\mathrm{FD}} := \lambda \cos(\omega \Delta t/2), \tag{5.19}$$

and the discrete representation of the frequency is

$$\omega_{\Delta} = \omega^{\mathrm{D}}_{\mathrm{FD}} := \omega s_{\omega}.$$

We compare the phase error for the FEM-D1 to phase error for the JHT-D scheme. The phase error is plotted against values of $\omega\Delta t$ in the range $[0, \pi]$. We note that $\omega\Delta t = 2\pi/N_{\mathrm{ppp}}$, where N_{ppp} is the number of points per period and is related to the number of points per wavelength N_{ppw} via

$$N_{\mathrm{ppw}} = \nu N_{\mathrm{ppp}}. \tag{5.20}$$

Thus, for $\nu \leq 1$, the number of points per wavelength is always less than or equal to the number of points per period, and conversely for $\nu > 1$. Note that the number of points per wavelength in the range $[\pi/4, \pi]$ is 8 to 2 points per period. We are more interested in the range $[0, \pi/4]$, which involves more than 8 points per period (or equivalently more than 8 points per wavelength).

To generate the plots below we have used the values given in (4.16), namely: $\epsilon_{\infty} = 1, \epsilon_s = 78.2$, and $\tau = 8.1 \times 10^{-12}$. Figure 8 plots the phase error Φ versus $\omega\Delta t$ for the FEM-D1 scheme (left), and the log of the phase error versus ω (right), using $h_\tau = 0.001$ and various values of ν. In Fig. 8 (right) we can see that in the finite element scheme, for a fixed frequency, the phase error reduces as ν increases, even beyond $\nu = 1$. We note that there is little difference for ν values larger than 4, thus we can restrict ourselves to $\nu \in (0, 4]$ in considering the best choices of ν to minimize dispersion. Figure 9 depicts the corresponding plots for the JHT-D method (recall JHT-D is conditionally stable for $\nu \leq 1$). We note that $\omega\Delta t = \pi$ corresponds to $N_{ppw} = 2$ in the case of $\nu = 1$, thus, this case in the left plot of Fig. 9 suggests that the JHT-D scheme has low dispersion even when the wavelength is very poorly resolved. However, the right plots of Figs. 8 and 9 show that FEM-D1 with large ν is superior in the frequency range near $1/\tau$.

The report [36] contains plots of the real and imaginary parts of the relative complex permittivity for Debye media corresponding to the continuous equations (exact values), the FEM-D1 scheme with $\nu \in \{\sqrt{1/2}, 1, 4\}$, $h_\tau \in \{0.1, 0.01\}$, and finally the JHT-D scheme with $\nu \in 1$ fixed and $h_\tau \in \{0.1, 0.01\}$. Figure 10 depicts a representative example. For $h_\tau = 0.1$, as ν is increased the discrete permittivities of the finite element scheme approach the exact values. For $h_\tau = 0.01$, the agreement of the discrete permittivities with the exact values is better than with $h_\tau = 0.1$, for each value of ν. For $\nu = 4$ we see the best agreement of the discrete real and imaginary permittivities with the exact values. For $\nu = 4$ we also see the best agreement of the discrete values of the parameters λ and ϵ_s with the exact values (see plots in [36]). However, the discrete value of the frequency ω for the FEM-D1, as shown in Fig. 11, appears to have a better agreement with the exact value when $\nu = 1$, even better than the finite difference scheme.

The discrete parameters in the FEM-D1 scheme have better agreement with the exact values as ν increases and h_τ decreases. For the JHT-D scheme, the discrete parameters do not depend on the value of ν. Still, as h_τ is decreased they do converge toward the exact values.

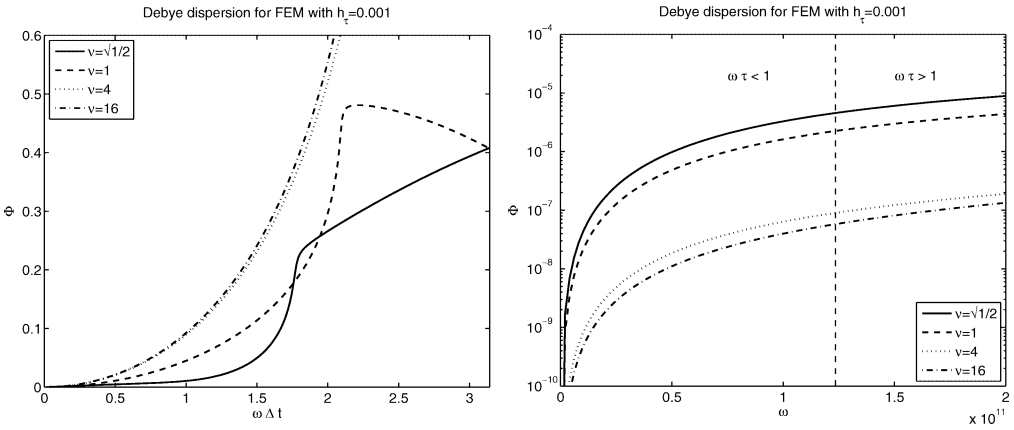

FIG. 8. Plot on left (right) is of the phase error Φ (resp., log of Φ) versus $\omega\Delta t$ (resp., ω) for the FEM-D1 scheme with $\nu \in \{\sqrt{1/2}, 1, 4, 16\}$ using $h_\tau = 0.001$.

For the particular values tested there, it appears that the value of ν that correctly represents λ will sufficiently model the entire complex permittivity for many frequencies. Thus our guideline for Debye media is to choose this value of the Courant number ν.

C. Lorentz Media

The dispersion relation for the continuous Lorentz model (with $\epsilon_\infty = 1$) is given by

$$k_{\mathrm{EX}}^{\mathrm{L}}(\omega) = \frac{\omega}{c}\sqrt{\epsilon_r^{\mathrm{L}}(\omega)}, \tag{5.21}$$

where the relative complex permittivity for Lorentz media is given to be

$$\epsilon_r^{\mathrm{L}}(\omega) := \frac{\omega^2 - \epsilon_s\omega_0^2 + i\lambda\omega}{\omega^2 - \omega_0^2 + i\lambda\omega}. \tag{5.22}$$

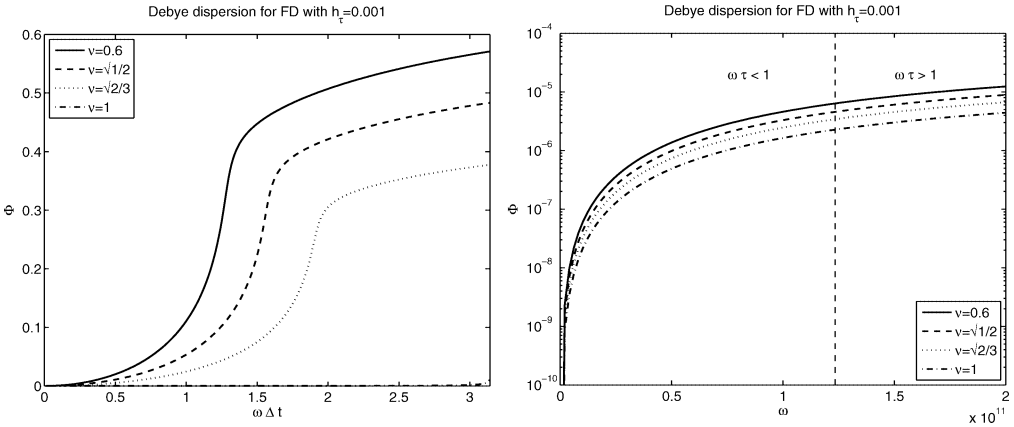

FIG. 9. Plot on left (right) is of the phase error Φ (resp., log of Φ) versus $\omega\Delta t$ (resp., ω) for the JHT-D scheme with $\nu \in \{1, \sqrt{2/3}, \sqrt{1/2}, .6\}$ using $h_\tau = 0.001$.

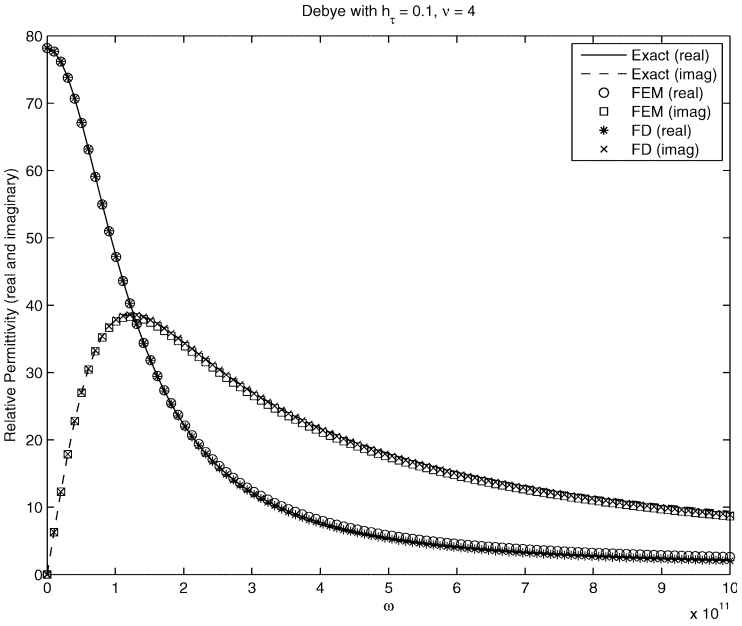

FIG. 10. Plots of the real and imaginary parts of the relative complex permittivity for Debye media corresponding to the continuous equations, the FEM-D1 scheme with $\nu = 4, h_\tau = 0.1$ and the JHT-D scheme with $\nu = 1, h_\tau = 0.1$.

As done for the Debye case, we will show below that the numerical dispersion relations for the finite element method as well as the FDTD method applied to Lorentz media can be written in the form

$$k_\Delta^{\mathrm{L}}(\omega) = \frac{2}{\Delta z} \sin^{-1}\left[\frac{\omega_\Delta}{c}\frac{\Delta z}{2}\sqrt{\epsilon_{r,\Delta}^{\mathrm{L}}}\right], \tag{5.23}$$

where the discrete relative complex permittivity is given to be

$$\epsilon_{r,\Delta}^{\mathrm{L}} := \frac{\omega_\Delta^2 - \epsilon_{s,\Delta}\omega_{0,\Delta}^2 + i\lambda_\Delta\omega_\Delta}{\omega_\Delta^2 - \omega_{0,\Delta}^2 + i\lambda_\Delta\omega_\Delta}. \tag{5.24}$$

To determine the numerical dispersion relation for the finite element method applied to a Lorentz medium (FEM-L) described in "Lorentz Media (FEM-L)" section, we substitute

$$X_j^n = \begin{bmatrix} e_j^n \\ p_j^n \\ d_j^n \\ q_j^n \end{bmatrix} = \begin{bmatrix} \tilde{e} \\ \tilde{p} \\ \tilde{d} \\ \tilde{q} \end{bmatrix} \mathrm{e}^{i(k_\Delta j\Delta z - \omega n\Delta t)}$$

into the discrete Eq. (3.8) with $\bar{M} = \bar{M}^{\mathrm{L}}, \bar{K} = \bar{K}^{\mathrm{L}}$ and $\bar{J} = \bar{J}^{\mathrm{L}}$ as given in (3.19)–(3.20) (with $B \equiv 0, J \equiv 0$).

As before we obtain a homogeneous system of the type $\mathcal{A}\tilde{\mathcal{X}} = 0$. We then set $\det(\mathcal{A}) = 0$ to obtain a relation between the numerical wavenumber k_Δ and the frequency ω. Solving for k_Δ in

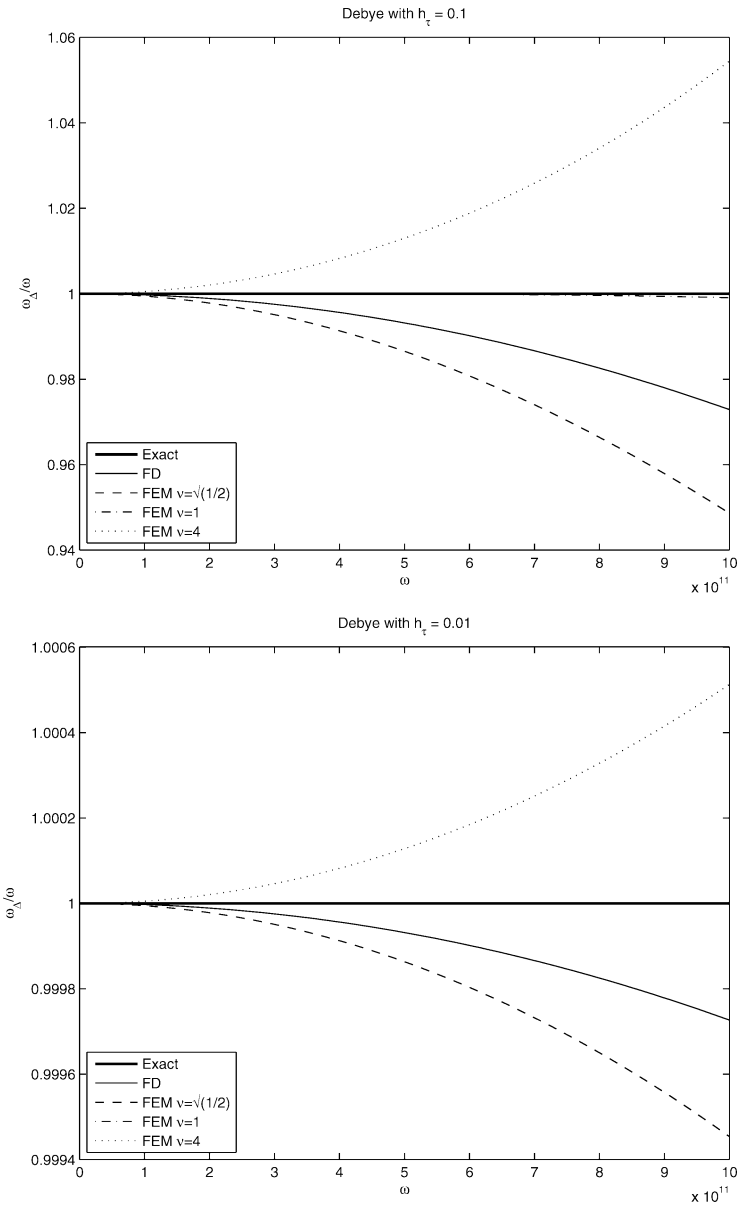

FIG. 11. Plots of the ratio of the discrete frequency ω_Δ for Debye media and the exact frequency ω, corresponding to the continuous equations, the FEM-D1 scheme and the JHT-D scheme (using $\nu = 1$) with $h_\tau = 0.1$ (left) and $h_\tau = 0.01$ (right). Note: in the right plot, the curve corresponding to FEM-D1 with $\nu = 1$ coincides with the exact curve to graphical resolution.

this relation, we have that the numerical dispersion relation for the FEM-L scheme is given by (5.23) with $k_\Delta^{\mathrm{L}} = k_{\mathrm{FE}}^{\mathrm{L}}$ the discrete relative complex permittivity given by (5.22) with $\epsilon_{r,\Delta}^{\mathrm{L}} = \epsilon_{r,\mathrm{FE}}^{\mathrm{L}}$, and the discrete medium parameters given by

$$\epsilon_{s,\Delta} = \epsilon_{s,\mathrm{FE}}^{\mathrm{L}} := \frac{\epsilon_s}{\alpha^2\beta^2} \tag{5.25}$$

$$\lambda_\Delta = \lambda_{\mathrm{FE}}^{\mathrm{L}} := \lambda \cos(\omega \Delta t/2)\alpha \tag{5.26}$$

$$\omega_{0,\Delta} = \omega_{0,\mathrm{FE}}^{\mathrm{L}} := \omega_0 \cos(\omega \Delta t/2)\beta\alpha^2 \tag{5.27}$$

$$\omega_\Delta = \omega_{\mathrm{FE}}^{\mathrm{L}} := \omega s_\omega \alpha, \tag{5.28}$$

where s_ω, α, β are as defined in Eqs. (5.14)–(5.16). Thus, the FEM-L scheme misrepresents ϵ_s, λ, ω_0, and ω as $\epsilon_{s,\mathrm{FE}}^{\mathrm{L}}$, $\lambda_{\mathrm{FE}}^{\mathrm{L}}$, $\omega_{0,\mathrm{FE}}^{\mathrm{L}}$, and $\omega_{\mathrm{FE}}^{\mathrm{L}}$ respectively. In particular, note that for the finite element method applied to the Lorentz model, $\lambda_{\mathrm{FE}}^{\mathrm{L}}$ does not depend on the continuous model parameter ϵ_s, however, $\omega_{0,\mathrm{FE}}^{\mathrm{L}}$ does. In the FEM-D1 scheme for the Debye model, $\lambda_{\mathrm{FE}}^{\mathrm{D}}$ depended on β^2, whereas in the FEM-L scheme for the Lorentz model, $\omega_{0,\mathrm{FE}}^{\mathrm{L}}$ depends directly on β. The square of the discrete parameter $\omega_{0,\Delta} = \omega_{0,\mathrm{FE}}^{\mathrm{L}}$ appears in the dispersion relation (5.23)–(5.24), so the contribution from β is again raised to the second power. This coupled with the fact that in the regime of interest $\omega \Delta t$ is small, implies that as before the effect of ϵ_s on the dispersion is likely to be small.

We compare the FEM-L scheme with two different finite difference schemes which have been analyzed in [7]. For the JHT-L scheme in [12] the numerical dispersion relation can be written in the form of (5.23)–(5.24) where the discrete representations of the continuous model parameters and the frequency are given as

$$\epsilon_{s,\Delta} = \epsilon_{s,\mathrm{JHT}}^{\mathrm{L}} := \epsilon_s \tag{5.29}$$

$$\lambda_\Delta = \lambda_{\mathrm{JHT}}^{\mathrm{L}} := \lambda \frac{\tilde{s}_\omega}{s_\omega} \tag{5.30}$$

$$\omega_{0,\Delta} = \omega_{0,\mathrm{JHT}}^{\mathrm{L}} := \omega_0 \sqrt{\cos(\omega \Delta t)} \tag{5.31}$$

$$\omega_\Delta = \omega_{\mathrm{JHT}}^{\mathrm{L}} := \omega s_\omega, \tag{5.32}$$

with $\tilde{s}_\omega = \frac{\sin(\omega \Delta t)}{\omega \Delta t}$.

The second finite difference scheme, the KF-L scheme of [14], has a numerical dispersion relation in the form of (5.23)–(5.24) given by the following discrete representations of the continuous model parameters and the frequency

$$\epsilon_{s,\Delta} = \epsilon_{s,\mathrm{KF}}^{\mathrm{L}} := \epsilon_s \tag{5.33}$$

$$\lambda_\Delta = \lambda_{\mathrm{KF}}^{\mathrm{L}} := \lambda \cos(\omega \Delta t/2) \tag{5.34}$$

$$\omega_{0,\Delta} = \omega_{0,\mathrm{KF}}^{\mathrm{L}} := \omega_0 \cos(\omega \Delta t/2) \tag{5.35}$$

$$\omega_\Delta = \omega_{\mathrm{KF}}^{\mathrm{L}} := \omega s_\omega. \tag{5.36}$$

We plot the phase error Φ as defined in (5.6) for the FEM-L method and we compare it with the phase errors for the JHT-L and the KF-L finite difference schemes. The phase error is plotted against values of $\omega \Delta t$ in the range $[0, \pi]$. We note that, as before, $\omega \Delta t = 2\pi / N_{\mathrm{ppp}}$ where again N_{ppp} is the number of points per period and is related to the number of points per wavelength N_{ppw} via (5.20).

To generate the plots below we have used the values for the medium parameters as given in (4.23). Figure 12 plots the phase error Φ versus ω for the FEM-L scheme, with various values of ν and using $h_0 = 0.01$. In this figure, note that the dispersion for the finite element method reduces as ν goes to 1 for all values of h_0. Figure 13 plots the phase error Φ versus ω for the KF-L scheme, with various values of ν and using $h_0 = 0.01$. We see that for low frequencies, the

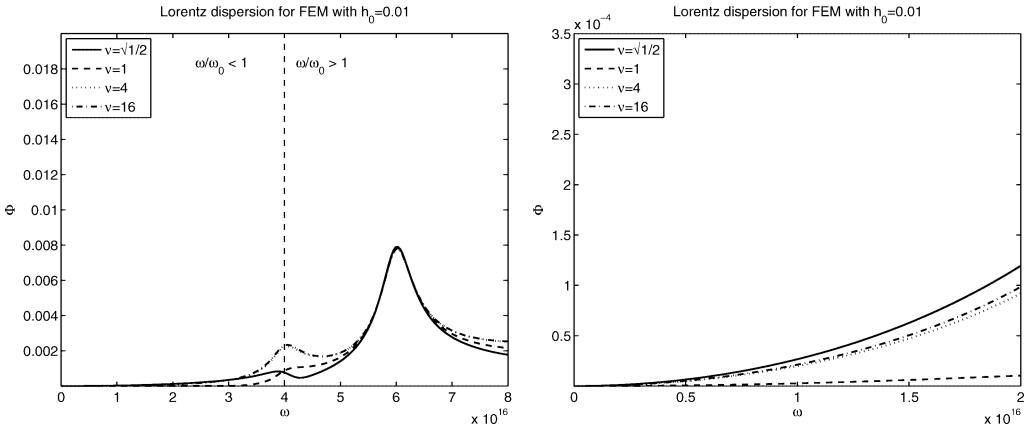

FIG. 12. Plot of the phase error Φ versus ω for the FEM-L scheme with $\nu \in \{\sqrt{1/2}, 1, 4, 16\}$ using $h_0 = 0.01$. (Right plot is zoom of left.)

FEM-L scheme has less dispersion by an order of magnitude than the KF-L scheme. Plots of the JHT-L scheme show that it is even worse (see [36]).

The report [36] also contains plots of the real and imaginary parts of the relative complex permittivity for Lorentz media corresponding to the continuous equations (exact values), the FEM-L scheme with $\nu \in \{\sqrt{1/2}, 1, 4, 16\}$, $h_0 \in \{0.1, 0.01\}$, and finally the KF-L scheme with $\nu = 1$ fixed and $h_0 \in \{0.1, 0.01\}$ (plots of JHT-L were similar and were thus omitted). See Figure 14 for a representative example in the case of $\nu = 1, h_0 = 0.1$. For $h_0 = 0.1$, as ν is increased, the discrete permittivities of the FEM-L scheme approach those of the KF-L method. However, for $\nu = 1$ it appears that *the finite element approximation is noticeably better*. For $h_0 = 0.01$, the agreement of the discrete permittivities with the exact values is better than with $h_0 = 0.1$, for each value of ν. For $\nu = 1$ we see the best agreement of the discrete real and imaginary permittivities with the exact values, regardless of h_0. This is not seen in the plots of the discrete values of the parameters λ, ϵ_s and ω_0 (for example, see Fig. 15 for ω_0 and [36] for other plots). The discrete parameters in the FEM-L scheme have better agreement with the exact values as ν is increased, even beyond

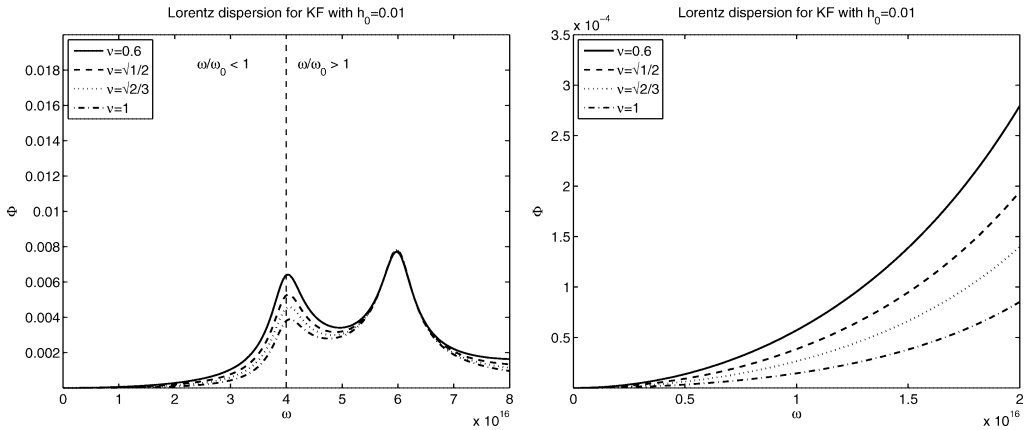

FIG. 13. Plot of the phase error Φ versus ω for the KF-L scheme with $\nu \in \{0.6, \sqrt{1/2}, \sqrt{2/3}, 1\}$ using $h_0 = 0.01$. (Right plot is zoom of left.)

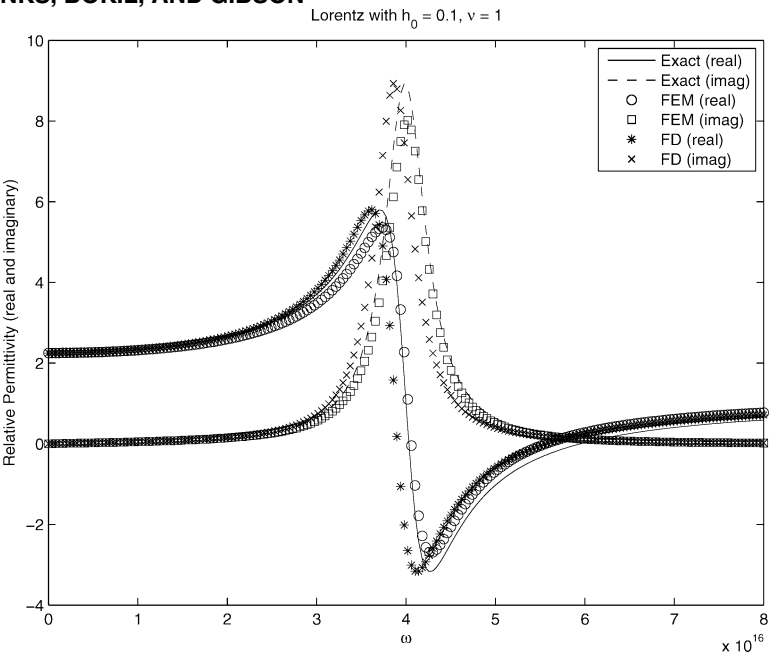

FIG. 14. Plots of the real and imaginary parts of the relative complex permittivity for Lorentz media corresponding to the continuous equations, the FEM-L scheme with $\nu = 1, h_0 = 0.1$ and the KF-L scheme with $\nu = 1, h_0 = 0.1$.

1. However the discrete value of the frequency ω appears to have a better agreement with the exact value when $\nu = 1$ (the plot is similar to that of Fig. 11 for the Debye case, and therefore is omitted).

As the discrete complex permittivity matches the exact more closely when $\nu = 1$, we conclude that for the Lorentz model, the value of ν that correctly represents ω will sufficiently model the complex permittivity and this is our guideline for Lorentz media. For the finite difference schemes, the discrete parameters do not depend on the value of ν. However, as with the finite element method FEM-L, if h_0 is decreased all discrete parameters agree better with the exact values. It should be noted that for the FEM-L scheme, as ν increases, the discrete parameters actually converge toward the KF-L values for fixed h_τ. Thus, if h_τ is too large for the KF-L values to have converged, the FEM-L scheme may actually have better agreement with the continuous values. This is precisely what is occurring in Fig. 14.

VI. NUMERICAL SIMULATIONS

To further compare and verify the observations drawn from the stability and dispersion analyses in the previous sections, we examine simulations of a sample problem using the Lorentz polarization model (the Debye model problem is verified in [36]). In our simulations, we successively reduce the value of h_τ, and hence the time step, holding all other parameters fixed, until convergence is achieved.

For interrogation of a Lorentz medium, we simulate the propagation of 12 cycles of a truncated sine wave with carrier frequency at 1.5 PHz (1.5×10^{15} Hz), which is normally incident on the

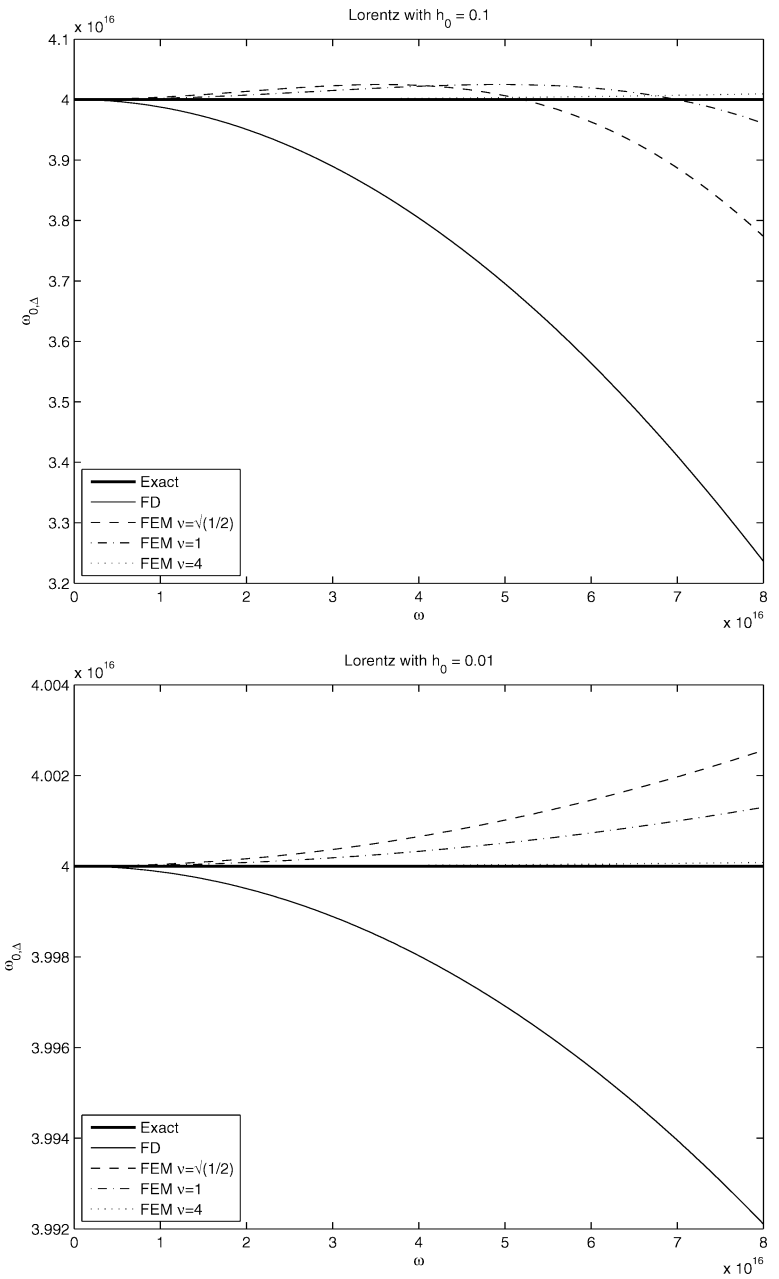

FIG. 15. Plots of the resonant frequency ω_0 for Lorentz media corresponding to the continuous equations, the FEM-L scheme and the KF-L scheme (using $\nu = 1$) with $h_0 = 0.1$ (left) and $h_0 = 0.01$ (right).

medium from a vacuum. The medium is defined by the parameters given in (4.23). We performed simulations with the finite element scheme, FEM-L, using $\nu = 1$.

A time trace of the electric field at a depth of 0.01 mm into the Lorentz medium was recorded. The left plot of Fig. 16 displays a close view of the central portion of the signal and demonstrates

that true convergence has not been reached. The right plot of Fig. 16 displays a magnification of one of the peaks from the central portion of the signal computed with smaller h_0 values. From this plot we can see that at most $h_0 = 0.02$ (i.e., at least 50 points per ω_0) is necessary for convergence on this small scale. The required value of $h_0 < 0.02$ is in line with the suggested range of $O(10^{-2})$.

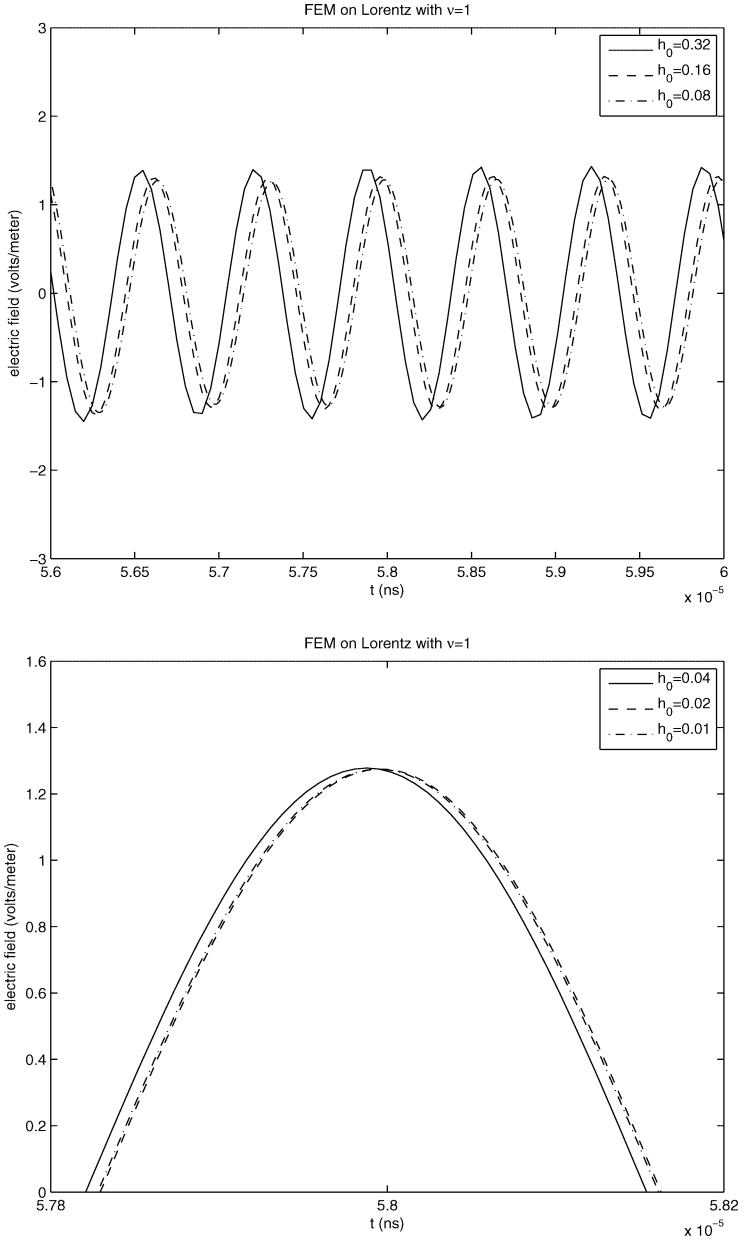

FIG. 16. Views of the center of the time trace of the electric field at a depth of 0.01 mm into a Lorentz medium (frequency is 1.5 PHz), for increasingly smaller values of h_0. (Right plot, using smaller values of h_0, is at a finer scale than the left plot.) Convergence is achieved at $h_0 = 0.02$.

VII. CONCLUSIONS

In this article, we have provided a stability and dispersion analysis and representative simulations of finite element schemes for modeling dispersive wave propagation in complex dielectric media. We considered materials described by Debye and Lorentz polarization models, but the numerical approach is sufficiently general to allow for any model with an ODE representation. We have contrasted our analyses with those corresponding to the finite difference schemes. From the stability and dispersion analysis as well as the simulations shown in the paper, we can conclude that the artificial dissipation in the FEM schemes presented here for Debye and Lorentz media are strongly dependent on the quantity $h_\tau = \Delta t/\tau$ when τ is the smallest time scale. For Lorentz media, in addition, the quantity $h_0 = \Delta t/T_0$ may be the dominant quantity if $T_0 = 2\pi/\omega_0$ is smaller than τ. We see that h_τ or h_0 have to be sufficiently small in order to accurately model the propagation of pulses at large distances inside the dispersive dielectric medium. For Debye media h_τ is recommended to be at least 100 points per τ, preferably $h_\tau = O(10^{-3})$. For Lorentz media we recommend either h_0 or h_τ to be $O(10^{-2})$ to minimize dissipation. These results are exactly the same guidelines for FDTD schemes posed in [7].

From the dispersion analysis for the finite element schemes we see that the value of the Courant number ν to be preferred is the one that provides the best agreement of the discrete relative complex permittivity with the exact permittivity, i.e., the value that results in the least phase error for the regime of interest. The unconditional stability of the FEM scheme allows the user to have some freedom in the choice of ν. For the Debye model, the value of ν that results in the best discrete representation of $\lambda = 1/\tau$ should sufficiently approximate the complex permittivity. For the Lorentz model, the value of ν that correctly represents the angular frequency ω should be chosen. For the FDTD scheme, however, conditional stability restricts the choice of $\nu = 1$ to minimize dispersion.

It is not straight-forward to say which of the methods has the best accuracy overall, as the distinction is heavily case dependent. However, for the particular case of relatively low frequency (as compared to other scales in the problem), and sufficiently fine mesh parameters, the analysis here has shown that the FEM schemes considered will have less dispersion than the FDTD methods for both Debye and Lorentz problems. Still, this does not take into account the increased computational cost of the FEM. The report [36] compares the stability and phase errors of the FEM schemes and the FDTD schemes for values of h_τ (and h_0) which result in comparable computational run times. In both the Debye and Lorentz cases, the stability results and phase errors for the FEM schemes considered are all on the same order of magnitude as in the FDTD methods.

Finally, finite element approaches allow the use of general meshes that can be used to avoid the stair stepping inaccuracies of the FDTD method in the modeling of complicated geometries. This along with unconditional stability and equivalent accuracy (to FDTD) makes the FEM a very attractive method for modeling dispersive wave phenomenon.

References

1. R. A. Albanese, R. L. Medina, and J. W. Penn, Mathematics, medicine and microwaves, Inverse Prob 10 (1994), 995–1007.

2. R. A. Albanese, J. W. Penn, and R. L. Medina, Short-rise-time microwave pulse propagation through dispersive biological media, J Opt Soc Am A 6 (1989), 1441–1446.

3. E. C. Fear, P. M. Meaney, and M. A. Stuchly, Microwaves for breast cancer detection, IEEE Potentials (2003), 12–18.

4. A. Taflove and S. C. Hagness, Computational electrodynamics: the finite-difference time-domain method, 3rd edition, Artech House, Norwood, MA, 2005.

5. P. Monk, A comparison of three mixed methods for the time-dependent Maxwell's equations, SIAM J Sci Stat Comput 13 (1992), 1097–1122.

6. J.-F. Lee, R. Lee, and A. Cangellaris, Time-domain finite element methods, IEEE Trans Antennas Propagat 45 (1997), 430–442.

7. P. Petropoulos, Stability and phase error analysis of FDTD in dispersive dielectrics, IEEE Trans Antennas Propagat 42 (1994), 62–69.

8. K. P. Prokopidis, E. P. Kosmidou, and T. D. Tsiboukis, An FDTD algorithm for wave propagation in dispersive media using higher-order schemes, J Electromagn Waves Appl 18 (2004), 1171–1194.

9. N. S. Stoykov, T. A. Kuiken, M. M. Lowery, and A. Taflove, Finite element time-domain algorithms for modeling linear Debye and Lorentz dielectric dispersions at low frequencies, IEEE Trans Biomed Enggr 50 (2003), 1100–1106.

10. R. Lee and A. C. Cangellaris, A study of discretization error in the finite element approximation of wave solutions, IEEE Trans Antennas Propagat 40 (1992), 542–549.

11. F. Edelvik and B. Strand, Frequency dispersive materials for 3-d hybrid solvers in time domain, IEEE Trans Antennas Propagat 51 (2003), 1199–1205.

12. R. M. Joseph, S. C. Hagness, and A. Taflove, Direct time integration of Maxwell's equations in linear dispersive media with absorption for scattering and propagation of femtosecond electromagnetic pulses, Opt Lett 16 (1991), 1412–1414.

13. T. Kashiwa, N. Yoshida, and I. Fukai, A treatment by the finite-difference time domain method of the dispersive characteristics associated with orientational polarization, IEEE Transactions IEICE 73 (1990), 1326–1328.

14. T. Kashiwa and I. Fukai, A treatment by the FD-TD method of the dispersive characteristics associated with electronic polarization, Microwave Opt Technol Lett 3 (1990), 203–205.

15. R. Luebbers, F. P. Hunsberger, K. S. Kunz, R. B. Standler, and M. Schneider, A frequency dependent finite-difference time-domain formulation for dispersive materials, IEEE Trans Electromag Compat 32 (1990), 222–227.

16. R. Luebbers and F. P. Hunsberger, FDTD for Nth-order dispersive media, IEEE Trans Antennas Propagat, 40 (1992), 1297–1301.

17. D. Kelley and R. Luebbers, Piecewise linear recursive convolution for dispersive media using FDTD, IEEE Trans Antennas Propagat 44 (1996), 792–797.

18. D. Sullivan, Z-transform theory and the fdtd method, IEEE Trans Antennas Propagat 44 (1996), 28–34.

19. D. Sullivan, A frequency-dependent FDTD method for biological applications, IEEE Trans Microwave Theory 40 (1992), 532–539.

20. I. Barba, A. C. L. Cabeceira, M. Panizo, and J. Represa, Modelling dispersive dielectrics in TLM method, Int J Numer Model 14 (2001), 15–30.

21. J. L. Young and R. O. Nelson, A summary and systematic analysis of FDTD algorithms for linearly dispersive media, IEEE Antennas Propag Mag 43 (2001), 61–77.

22. R. Siushansian and J. LoVetri, A comparison of numerical techniques for modeling electromagnetic dispersive media, IEEE Microwave Guided Wave Lett 5 (1995), 426–428.

23. B. Bidegaray-Fesquet, Stability of FD-TD schemes for Maxwell-Debye and Maxwell-Lorentz equations, Laboratoire de Modélisation et de Calcul, CNRS, 2005.

24. S. A. Cummer, An analysis of new and existing FDTD methods for isotropic cold plasma and a method for improving their accuracy, IEEE Trans Antennas Propagat 45 (1996), 392–400.

25. H. T. Banks, M. W. Buksas, and T. Lin, Electromagnetic material interrogation using conductive interfaces and acoustic wavefronts, Vol FR21 of Frontiers in applied mathematics, SIAM, Philadelphia, PA, 2000.

26. H. T. Banks, N. L. Gibson, and W. P. Winfree, Gap detection with electromagnetic terahertz signals, Technical Report CRSC-TR03-40, Center for Research in Scientific Computation, September, 2003, Nonlinear Anal: Real World Applications, 6 (2005), 381–416.

27. R. A. Albanese, H. T. Banks, and J. K. Raye, Nondestructive evaluation of materials using pulsed microwave interrogating signals and acoustic wave induced reflections, Inverse Prob 18 (2002), 1935–1958.

28. J. C. Strikwerda, Finite Difference Schemes and Partial Differential Equations, SIAM, 2004.

29. J. D. Jackson, Classical electromagnetics, Wiley, New York, 1999.

30. H. T. Banks and N. L. Gibson, Electromagnetic inverse problems involving distributions of dielectric mechanisms and parameters, Technical Report CRSC-TR05-29, Center for Research in Scientific Computation, August, 2005, Quarterly Appl Mathe, 64 (2006), 749–795.

31. J. C. Anderson, Dielectrics, Chapman and Hall, London, 1967.

32. K. S. Cole and R. H. Cole, Dispersion and absorption in dielectrics, J Chem Phy 9 (1941), 341–351.

33. H. T. Banks and N. L. Gibson, Well-posedness in Maxwell systems with distributions of polarization relaxation parameters, Technical Report CRSC-TR04-01, Center for Research in Scientific Computation, January, 2004, Appl Math Lett, 18 (2005), 423–430.

34. P. Debye, Chemical Catalog, New York, 1929.

35. R. L. Burden, J. D. Faires, Numerical Analysis, PWS, Boston, 1993.

36. H. T. Banks, V. A. Bokil, and N. L. Gibson, Analysis of stability and dispersion in a finite element method for Debye and Lorentz dispersive media, Technical Report CRSC-TR06-21, Center for Research in Scientific Computation, August, 2006.

37. N. L. Gibson, Terahertz-based electromagnetic interrogation techniques for damage detection, PhD Thesis, N. C. State University, Raleigh, 2004.

38. K. E. Oughstun and G. C. Sherman, Uniform asymptotic description of electromagnetic pulse propagation in a linear dispersive medium with absorption (the Lorentz Medium), J Opt Soc Am A 6 (1989), 1394–1420.

39. A. Taflove, Computational electrodynamics: the finite-difference time-domain method, Artech House, Norwood, MA, 1995.